

Manuscript Template

2	Title	
3		Multiple carbon incorporation strategies support microbial survival in
4		cold subseafloor crustal fluids
5		
6	Autho	ors
7		Elizabeth Trembath-Reichert ¹ *, Sunita R. Shah Walter ² , Marc Alec Fontánez Ortiz ³ ,
8		Patrick D. Carter ⁴ , Peter R. Girguis ⁵ , and Julie A. Huber ⁶
9		.•
10	Affilia	ntions
11 12		¹ School of Earth and Space Exploration, Arizona State University, Tempe, AZ, 85287
13 14		² School of Marine Science & Policy, University of Delaware, Lewes, DE, 19958
15		³ School of Life Sciences, Arizona State University, Tempe, AZ, 85287
16		45
17 18		⁴ Department of Microbiology, University of Massachusetts, Amherst, MA, 01003
19		⁵ Organismic and Evolutionary Biology, Harvard University, Cambridge, MA, 02138
20		organismic and Evolutionary Biology, that vard only orototy, Camoriago, 1411, 02130
21		⁶ Marine Chemistry & Geochemistry, Woods Hole Oceanographic Institution, Woods
22		Hole, MA, 02543
23		
24		*Correspondence to: e.t.r@asu.edu
25		
26	Abstr	act
27	Bioge	ochemical processes occurring in fluids that permeate oceanic crust make measurable
28	contril	butions to the marine carbon cycle, but quantitative assessments of microbial impacts on
29		st, subsurface carbon pool are lacking. We provide bulk and single cell estimates of
30		bial biomass production from carbon and nitrogen substrates in cool, oxic basement fluids
31		he western flank of the Mid-Atlantic Ridge. The wide range in carbon and nitrogen
32		oration rates indicates a microbial community well-poised for dynamic conditions,
33		ially anabolizing carbon and nitrogen at rates ranging from those observed in subsurface
34		ents to those found in on-axis hydrothermal vent environments. Bicarbonate incorporation
35		were highest where fluids are most isolated from recharging bottom seawater, suggesting
36	that ar	nabolism of inorganic carbon may be a potential strategy for supplementing the ancient and

40 Quanti

3738

41 42

43

Quantitative assessments of microbial activity in crustal fluids yield potential strategies to supplement recalcitrant DOC.

recalcitrant DOC that is prevalent in the globally-distributed subseafloor crustal environment.

Introduction

In the deep ocean, seawater is entrained into the rocky crust, chemically altered by abiotic and microbial processes, and discharged from the seafloor as hydrothermal fluid with a global flux that rivals riverine inputs (1, 2). Over 90% of this hydrothermal fluid discharge is from lowtemperature fluids $(5-20^{\circ}\text{C})$ circulating on the flanks of mid-ocean ridges (1), where these fluids are generally inaccessible and their microbial assemblages largely unexplored (3). The biogeochemical influence of this cool, ridge-flank microbiome on net chemical fluxes, and particularly on the enormous, climate-sensitive reservoir of deep-ocean DOC, is potentially significant, but poorly constrained. For this study, pristine, cool, basaltic subseafloor fluids (4) from 8 Ma crust were recovered from ocean drilling borehole observatories of the North Pond site located at 22 °N on the western flank of the mid-Atlantic Ridge. Here, oxygenated crustal fluids are largely indistinguishable from bottom seawater and concentrations of ammonium, methane, hydrogen sulfide, and iron (II) are below detection, indicating an overall low redox energy potential in these subseafloor crustal fluids (5). While DOC sourced from the deep ocean is thought to be unreactive and resistant to microbial degradation (6, 7), previous isotopic data from these fluids suggest selective removal of DOC via microbial oxidation does occur (8, 9) and DOC may, therefore, be the most abundant reduced substrate available for microbes to oxidize in cool crustal fluids (9).

While the abundance and diversity of microorganisms in the subseafloor has been explored for decades via scientific drilling programs (10), slow growth, and often low biomass, present challenges for demonstrating microbial activity under environmentally relevant conditions. Microbial activity via uptake of labeled substrates has been successfully observed in sedimentary (11-13) and diffuse flow hydrothermal vent fluids (14-16) using stable isotope probing (SIP) incubations coupled to single cell measurements with nanoscale secondary ion mass spectrometry (NanoSIMS), providing constraints on the potential microbial contribution to primary production and organotrophy in these habitats. However, no such data exist from the crustal biome. Here we determine single cell and bulk estimates of microbial carbon and nitrogen incorporation from the ridge flank crustal habitat that represents the majority of fluid flux between the subsurface and the overlying ocean. Our extensive and quantitative assessments highlight a microbial population poised to incorporate fresh sources of labile organic carbon and a consistent, wide range of intercell incorporation rates across fluids and conditions. We also report significant bicarbonate incorporation, despite the absence of abundant inorganic sources of redox energy that could fuel chemolithotrophy, and suggest this may be part of a metabolic strategy of supplementing anabolic carbon needs with bicarbonate to reduce the reliance on aged and recalcitrant deep-ocean DOC.

installed in 2011 at IODP Sites U1382A and U1383C (Figure 1A). The CORK at site U1382A accesses circulating fluids from one depth interval below the sediment in the rocky subseafloor (90-210 mbsf), and the U1383C CORK accesses three depth ranges: Shallow (70-146 mbsf), Middle (146-200 mbsf), and Deep (200-332 mbsf). Although the geochemistry of fluids recovered from both CORK observatories are largely similar to overlying seawater, radiocarbon measurements and larger differences in dissolved oxygen and DOC concentrations indicate that fluids recovered from U1383C are more isolated from bottom water recharge than U1382A (5, 8, 9). Recent numerical simulations suggest there is convective and oscillatory fluid movement through the rocky crust (17), rather the simple linear flow along the north-south axis as had been hypothesized in earlier studies of North Pond (4).

North Pond hosts two CORK (Circulation Obviation Retrofit Kit) seafloor borehole observatories

Results and Discussion:

44

45

46

47

48

49

50 51

52

53

54

55

56 57

58

59

60

61

62

63

64 65

66

67

68

69

70

71

72

73

74

75

76

77

78

79 80

81

82

83

84

85 86

87 88 89

90

91

92

Fluids described in this study were collected using a mobile pumping system (18) in October 2017 as a part of the third sampling expedition to North Pond. Bottom seawater was also collected by Niskin bottles on a CTD sampling rosette. 16S rRNA gene sequencing of all samples (North

Pond crustal fluids and bottom seawater) indicates the microbial community in crustal fluids is distinct from those communities in bottom seawater in 2017 (Figure S1, S2), as has been seen in previous years (8, 19). Within the crustal fluids, the microbial community at U1382A is more similar to bottom water than the U1383C fluid horizons, which is also consistent with geochemical data (5). Moreover, in a separate study of a diverse range of mineral chips incubated in the CORKs for 4 to 6 years (retrieved in 2017), the authors recovered similar taxa across all sample types (CORK fluids, bottom water, and mineral chips) and determined that the incubation fluid explained more of the microbial community composition colonizing minerals than the type of mineral surface (20). Together these results indicate the fluids collected in 2017, and used in the current study, are capturing the dominant microbial communities in the North Pond crustal fluids.

93

94

95

96

97 98

99 100

101

102 103

104

105

106

107

108

109

110

111

112

113

114

115

116

117

118 119

120

121

122

123

124

125

126

127

128

129

130

Cell counts from CORK fluids in 2017 ranged from 2.1 to 5.1 x10³ cells ml⁻¹ (Table 1). These 2017 counts are lower than historical cell count data for previously collected fluids, which have ranged from high 10^3 to low 10^4 cells ml⁻¹ of fluid (8, 19). Decreasing cell concentrations post drilling has also been observed in other CORKs (Juan de Fuca ridge flank; 21) and groundwater well systems (22). Together with geochemical data (Table 1; 5), low cell counts likely indicate the North Pond system had recovered from drilling and that the 2017 fluids (and resulting data) are the best representation of microbial activity in the cold, oxic crustal subseafloor aguifer to date.

Incubations of bottom seawater and crustal fluids were all amended with deuterated (²H₂O) water, which can be used as a general tracer of microbial anabolic activity (23). Select combinations of ¹³C carbon (bicarbonate, acetate, methylamine, and diatom lysate) and ¹⁵N nitrogen (ammonium, methylamine, and diatom lysate) were provided as substrate-specific tracers of anabolic activity (Table 2). No substrates were added to CN controls. For diatom lysate, diatoms were grown in the presence of isotopically enriched ¹³C-bicarbonate and ¹⁵N-nitrate and then lysed prior to addition as a proxy for environmentally relevant complex organic matter. Incubations were conducted at temperatures bracketing the expected range in the North Pond aquifer (4°C to 20°C), and cells were harvested from separate incubations prepared for three time points (12 hr, 2 days, and 6 days; Table 2). Isotope incorporation rates were calculated from bulk elemental analysis (Figure 1B-D) and single cell NanoSIMS measurements (Figure 2, 3).

conditions. Cell counts from organic carbon amended incubations (acetate and diatom lysate) had the highest cell densities in earlier time points (Figure S3). By 2 days, all incubations with acetate (1383C Middle) or diatom lysate (all other samples) had the highest cell densities. By the final time point of 6 days, most of these organic carbon incubations had a lower cell density than earlier time points or CN controls, suggesting an initial period of cell growth followed by death. This pattern of cell increase in the first few days followed by decrease has also been observed in groundwater wells with no amendments (22), which the authors attribute to necromass induced growth from cells that die off at the onset of the incubation.

Microbial populations in North Pond fluids appear poised for dynamic and heterogeneous

- In bulk analysis performed on ¹³C-acetate, ¹³C-methylamine, and ¹³C-bicarbonate amended 131 incubations, acetate incorporation was widespread across fluids and conditions (Figure 1B). 132 Bicarbonate incorporation was not detected as consistently as acetate incorporation, but was on 133 par with acetate incorporation in some fluids (e.g., U1383C Middle and Deep, Figure 1C). 134 Methylamine incorporation rates were lower overall, compared to acetate and bicarbonate, but 135 uniquely elevated in U1383C Middle at both 4°C and 20°C (Figure 1D). 136
- Bulk rates of carbon incorporation from acetate were highest at 6 days for all 20°C fluids except 137 U1383C Shallow, where the rate decreased between day 2 and 6 (Figure 1B). Acetate 4°C 138 139
 - incubations were generally lower than their 20°C counterparts (except for U1383C Shallow where

- incorporation (Figure 3A) showed a bimodal distribution of rates for U1383C Deep (20°C) and
- Shallow (4°C) at their respective *in situ* temperatures. These data suggest that microbes in deeper
- crustal fluids may persist on recalcitrant carbon sources, with select members poised to quickly
- respond to an influx of more labile organic carbon.
- Previous genomic studies of North Pond crustal fluid microbial communities collected in 2012
- recovered genes for autotrophic CO₂ fixation (8, 19), and much higher incorporation of ¹³C-
- bicarbonate than ¹³C-acetate (800 to 4,300 pmol ml⁻¹d⁻¹ vs. no more than 104 pmol ml⁻¹d⁻¹; Table
- 148 S4) from SIP incubations (8). However, the fluids collected in 2012, only 6 months after drilling,
- were particle-laden and geochemical data suggested they represented a mixture of crustal fluids,
- bottom seawater, and surface seawater (5). ¹³C-bicarbonate incorporation rates from 2017 CORK
- 151 fluids were much lower and ranged from below detection to 94 pmol ml⁻¹d⁻¹. 2017 bottom
- seawater rates (0.95 pmol ml⁻¹d⁻¹) were comparable to a study from the western branch of North
- Atlantic Deep Water, which overlays the North Pond site (0.24 pmol ml⁻¹d⁻¹ from ¹⁴C-
- bicarbonate, 2537 m water depth; Table S4)(24). Thus, it appears that bicarbonate incorporation
- may have been artificially elevated in these early studies.
- Still, bicarbonate incorporation rates on par with acetate incorporation in some 2017 fluids is
- surprising because of the lack of abundant electron donors typically used for chemolithotrophy.
- Though oxygen was abundant, methane, hydrogen sulfide, ammonium and reduced iron are all
- below detection limits (5, 8) and unlikely to fuel extensive autotrophic carbon fixation in North
- 160 Pond crustal fluids.
- Limited carbon fixation driven by the oxidation of reduced iron and sulfur minerals on basalt
- surfaces is still possible, although ¹³C-bicarbonate stable isotope incubations conducted with
- basalt samples and metagenomics investigations of these same rocks showed no conclusive
- evidence for carbon fixation (25, 26). However, global estimates indicate its importance in the
- 165 first ~10 Ma of crustal evolution (27) and chemolithotrophy in biofilms on rock surfaces may not
- have been captured by observations of bulk rates.
- 167 Given the lack of electron donors that could be paired with chemolithotrophy in our incubations,
- it is unlikely that rock-driven autotrophy is occurring in our experiments. Metagenomic and
- metatranscriptomic analysis of the same 2017 North Pond fluids used in our experiments showed
- more transcription of organic carbon utilizing pathway genes than autotrophic pathway genes
- across all sampling horizons, suggesting a microbial community engaged in organotrophy (28).
- 172 Carbon fixation transcripts were most abundant in 1383C Middle and Deep where we also
- detected the highest rates of bicarbonate incorporation. Furthermore, metagenomic-assembled
- genomes (MAGs) from the fluids revealed a number of MAGs contained carbon fixation
- pathways linked to oxidation of sulfide and thiosulfate, but these same MAGs also contained
- numerous extracellular protease and carbohydrate catabolism genes, consistent with a
- mixotrophic lifestyle.
- These North Pond results are in accordance with the predominance of heterotrophic bacteria
- 179 reported in ~33 and 104 Mya basalt crust cored beneath the South Pacific Gyre (29), as well as in
- subseafloor ultramafic and gabbroic rocks cored from the Atlantic Ocean (30, 31), where
- organotrophic microbial processes also dominate.
- Because DOC is the reduced substrate with the highest concentration in the North Pond crustal
- fluids (20-31 µmol/kg DOC; Table 1), organotrophy coupled with anabolism of both organic and
- inorganic carbon is the more likely explanation for observed uptake of bicarbonate. While
- anabolic incorporation of bicarbonate is underexplored in environmental settings, it has been
- demonstrated in laboratory conditions with pure cultures. For example, *Pseudomonas* AM1,
- 187 Hyphomicrobium vulgare, and Methylobacterium extorquens, are able to use a combination of the

Science Advances Manuscript Template Page 4 of 37

ethylmalonyl-CoA pathway and serine cycle, resulting in as much as 50% of biomass carbon derived from bicarbonate (32, 33).

We hypothesize organotrophy coupled to anabolism of both organic and inorganic carbon reflects microbial communities optimizing the low potential redox energy conditions in the rocky subseafloor. Crustal fluid DOC likely represents the fraction of deep ocean DOC that remains after the more bioavailable components are removed on short timescales after fluids are entrained in the crust (9). Our results indicate that this degraded DOC alone supports an active microbial population since cell growth was observed even when no carbon or nitrogen or other reduced substrates were added to incubations. DOC may be largely oxidized for energy by organotrophic pathways and bicarbonate may provide a supplementary, and less metabolically expensive, anabolic source of carbon.

Bicarbonate incorporation rates from 2017 were consistently high across time points in U1383C Deep fluids and highest with U1383C Middle fluids in 2 day incubations at 4°C and 20°C (Figure 1C). U1383C Middle and Deep fluids are also the fluids with the most "aged", or ¹⁴C-depleted DOC (9). DOC in fluids from U1383C has a radiocarbon age of 7,300 – 9,200 years and a higher aromaticity index and percent carboxyl-rich alicyclic molecules (CRAM) than bottom water or fluids from U1382A (9). Since DOC concentrations are lower at all subseafloor depths at U1383C compared to U1382A (Table 1), and compositional evidence indicates the DOC is the most aged and degraded at U1383C (9), microbial communities at this site may have the most to gain from supplementing their anabolic needs with bicarbonate incorporation. Our results indicate that there is not a concentration limit below which natural DOC is unavailable to microbes (34), but rather, there could be a different strategy for accessing the aged and recalcitrant fraction of deep-ocean DOC by combining biomass production from both inorganic and organic carbon sources (Figure S8). This could be supplemented by other oligotrophic strategies to utilize diverse sources of organic carbon in low DOC (<4 μM) conditions (35).

While dissolved nitrogen has been less studied at North Pond than DOC, ammonium loss through nitrification has been hypothesized in North Pond fluids based on geochemical fluxes (5). All of the provided nitrogen sources analyzed from U1383C Deep (15N-ammonium, 15N-methylamine, and 15N-diatom lysate) and U1383C Shallow fluids (15N-ammonium) were incorporated by cells based on NanoSIMS analysis (Figure 3B). It was generally observed that when 15N-ammonium was paired with 13C-acetate, the nitrogen incorporation rate was higher than when paired with 13C-bicarbonate. It was also observed that 13C and 15N diatom lysate C and N incorporation rates were similar to the 15N-ammonium and 13C-acetate C and N rates for comparable 12 hr 20°C U1383C Deep incubations. Therefore, organic nitrogen anabolic rates may have been higher when organic carbon was also provided (Table 3; Figure S8).

Methylamine incorporation was observed in all fluids. The highest methylamine incorporation rate (72 pmol C ml⁻¹d⁻¹) was from the same condition that had the highest bicarbonate incorporation rate, U1383C Middle 20°C at 2 days. This suggests Middle fluids were the most amenable to different carbon sources, with the highest rates of bicarbonate and methylamine carbon incorporation and the third highest acetate incorporation. Bulk carbon incorporation of methylamine was comparable to carbon uptake rates of other simple organic N compounds from oxygen deficient zones (ODZ) with similar oxygen concentrations to North Pond crustal fluids (*36*), such as urea and cyanate (5 to 12 and 2 to 14 pmol C ml⁻¹d⁻¹, respectively; Table S4). However, nitrogen incorporation rates from the same compounds in ODZ incubations ranged from 2 to 265 pmol N ml⁻¹d⁻¹, which were much higher than average nitrogen incorporation rates derived from single cell analysis of North Pond microbial communities (Table 3), where the highest average rate from diatoms was 6 pmol N ml⁻¹d⁻¹ and ammonium was 1 pmol ml⁻¹d⁻¹.

Science Advances Manuscript Template Page 5 of 37

Overall, this suggests that both C and N can be incorporated from organic N sources in North 237 238

Pond crustal fluids and from these organic N sources, North Pond C incorporation rates were

more similar to ODZ rates than the N incorporation rates.

239

240

241

242

243

244

245

246

247

248

249

250

251 252

253

254

255

256

257 258

259

260

261

262 263

264

265

266

267

268

269

276

278

279

280 281

282 283

284

Cool, crustal aquifer fluids appear to support a wider range of microbial activities than more stable subsurface sedimentary and diffuse flow hydrothermal vent counterparts. The average observed single cell uptake rates (10⁻³ to 10⁰ fmol C or N cell⁻¹d⁻¹; Table 3) fall between SIP-NanoSIMS rates derived from deep, organic-rich marine sediments incubated with bicarbonate and ammonium (10⁻² fmol C or N cell⁻¹d⁻¹; Table S5) and diffuse flow hydrothermal vent fluids of the East Pacific Rise incubated with bicarbonate (10⁰-10¹ fmol C cell⁻¹d⁻¹; Table S5). The highest average C and N North Pond incorporation rates were observed in 20°C incubations (U1383C Deep with acetate and ammonium at 1 fmol C cell⁻¹d⁻¹ and 0.1 fmol N cell⁻¹d⁻¹; U1383C Shallow with bicarbonate and ammonium at 3 fmol C cell⁻¹d⁻¹ and 0.4 fmol N cell⁻¹d⁻¹; Table 3). While the upper end of this range may only be observed under incubation conditions, the highest average rates were from incubations where no additional DOC was provided (bicarbonate amendments) and illustrates the potential for North Pond crustal microbes to exhibit high anabolic rates using aged DOC and little or no inorganic redox-active substrates for energy conservation. Higher bicarbonate uptake observed in the shallower fluids at 20°C may also be the result of supplemental bicarbonate anabolism, which allowed the colder in situ fluid community to more quickly take advantage of growth under warmer incubation temperatures, similar to deeper communities using bicarbonate to supplement available DOC. Therefore, in addition to implications for marine carbon and nitrogen cycling, the wide range in potential incorporation rates may have additional import for understanding evolutionary constraints in subseafloor

A global first-order estimate approximated 10¹¹-10¹² mol organic carbon could be incorporated per year in the cool subseafloor crustal aquifer fluids. This is derived from an estimated habitable pore volume for North Pond-age crust (<10 Ma) and the average single cell uptake rates from U1383C Shallow and Deep fluid incubations amended with organic carbon at the temperatures most relevant to *in situ* conditions (Table 4). This average estimate for fluid biomass production from organic carbon agrees with the estimated annual removal of DOC from cool crust at 10^{11} mol DOC year-1 (9) and suggests the majority of DOC loss could be associated with organotrophic and anabolic processes rather than catabolism. We also find organic nitrogen (average rates of 10¹⁰ to 10¹¹ mol N year⁻¹) may be anabolized per year in this system.

ecosystems, which have been heretofore been based on sedimentary and diffuse flow "end-

Estimates for bicarbonate incorporation were approximately 10^{10} - 10^{11} mol C year⁻¹ (Table 4) and 270 provide a potential mechanism for adding more labile, organic carbon to the crustal aquifer 271 (Figure S8). This estimate from young crustal fluids is higher than estimates of annual primary 272 productivity from hydrothermal systems at 10⁹ mol C year⁻¹ (24), suggesting cool crustal fluid 273 bicarbonate utilization may be equally or more significant than on-axis hydrothermal vent fluids 274 on a global scale. 275

Materials and Methods

member" subseafloor biomes.

277 Sample Collection

Fluids were collected from the basaltic aguifer at North Pond (22°45'N and 46°05'W) in October

2017 during cruise AT39-01 of the R/V Atlantis using ROV JASON II during expedition AT39-01.

Fluids were sampled from two CORK installations, each with umbilicals that are accessible at the

seafloor and terminate in a subsurface hydrologic zone: U1382A (includes one umbilical) and U1383C (includes 3 umbilicals; Shallow, Middle, and Deep; Table 1, Figure 1). Filtered samples

were collected using the mobile pumping system (MPS; 8, 37). Sample purity was evaluated by

monitoring geochemical parameters. Temperature and oxygen concentrations of the fluids were

continuously monitored using an inline optode oxygen/temperature sensor (Aanderaa, Bergen, Norway). Prior to filtering, umbilical lines were flushed until oxygen concentrations were stable and reached the expected values previous observed in each horizon. Then, crustal fluid was pumped at a rate of ~0.5 LPM for 80 min through a 0.22 μm, 47 mm GWSP filter (MilliporeSigma, Burlington, MA, USA). MPS sample purity has also been demonstrated at other CORK installations where the geochemistry of the crustal fluids is more distinct from seawater (21). Fluids were also minimally disturbed during recovery and kept in a narrow temperature range between sampling and incubations. In addition, bottom seawater was filtered and collected at 4,397 m water depth by holding the MPS pump inlet ~5 m off the seafloor and pumping for 80 min. All filters collected on the seafloor had a reservoir of RNAlaterTM (Ambion, Austin, TX, USA) that could weep into the filter for *in situ* fixation as described in (18). Upon recovery, filters were removed from the reservoirs and placed in fresh RNALaterTM, incubated at 4°C for 18 hours, and subsequently stored at -80°C shipboard.

Aguifer fluid was also collected by the MPS (~0.5 LPM for ~20 min) into multiple acid-washed custom 15 L TedlarTM bags for onboard SIP incubations and shipboard filtration. ~10 L was filtered in series to capture "particle-attached" (5 µm) and "free-living" (0.22 µm) fractions (47 mm GWSP, MilliporeSigma). TedlarTM bag fluids were transferred to SIP microcosms using a peristaltic pump, sterile acid-washed tubing, and sterile needles (for incubations). Bottom seawater for microcosms was collected by Niskin bottles via a CTD water sampling rosette to the same bottom seawater depth as the in situ MPS filter. These fluids were collected by bringing Niskin bottles into the laboratory and processed in the same manner as MPS bag fluids. Filtering on deck was carried out using the same filter holders with in situ fixation as those used on the seafloor.

DNA Extraction, 16S rRNA gene amplification, sequencing, and analyses

DNA was extracted using a phenol chloroform protocol (16) from in situ and onboard filters from all four CORK horizons (1382A and U1383C Shallow, Middle, and Deep) and the bottom seawater samples (MPS and CTD) and both filter size fractions. 16S rRNA gene amplicon libraries were prepared and sequenced by the UConn Microbial Analysis, Resources, and Services using modified EMP primers (38–41). 16S rRNA gene reads were processed using mothur (v.1.39.5; 38), and 97% similarity Operational Taxonomic Units (OTUs) were classified with the SILVA v128 database (42). A distance matrix of these OTUs was computed using Bray-Curtis dissimilarity with vegan (43). This matrix was then ordinated using classical multidimensional scaling with the R function *cmdscale* and clustered with the maximum allowable number of clusters (5) and membership exponent (1.5). For taxonomy figure generation, only OTUs greater than or equal to 0.5% of an individual sample were retained and R ggplot tools were used for display (44).

Stable Isotope Probing (SIP) Incubations

285

286

287

288

289 290

291 292

293 294

295

296

297 298

299

300

301

302

303 304

305

306

307

308 309

310

311

312

313

314

315

316

317

318

319 320

321

322 323

324

325

326

327

328

329

330

331

332

333

334

Incubations were prepared in 50 ml serum vials with labeled substrates prior to the cruise in acid washed and combusted glassware with crimped autoclaved butyl rubber stoppers. All serum vials contained 5 ml of 99.99% ²H₂O and carbon and nitrogen isotopes were added to a final concentration of 0.2 mM ¹³C-Sodium Bicarbonate, 1.5 μM ¹³C-Sodium Acetate (dual carbon label), 10 nM ¹⁵N-Ammonium Chloride, 4 μM ¹⁵N¹³C-Methylamine-HCl and estimated 2 μM ¹³C and 4 µM ¹⁵N from diatom lysate. ~45 ml of sample fluid was added to each vial for a total volume of 50 ml. All isotopes were from Cambridge Isotopes (Tewksbury, MA, USA). Controls with no C and N label were also included. After fluid addition to pre-labeled bottles, incubations were carried out for 12 hours, 2 days, or 6 days at either room temperature (~20°C, monitored during the cruise and remained within +/- 1°C of 19°C) or at 4°C in a walk-in refrigerator. 20°C

Science Advances Manuscript Template Page 7 of 37

- was chosen as the upper temperature limit because early temperature measurements from North
- Pond suggested basement temperatures up to 20°C at approximately 600 mbsf (45). 4°C was
- chosen as the lower temperature limit to represent the shallowest fluids at bottom water
- temperatures.

365

366

367

368

374

377

381

- While shipboard incubations inherently induce a variety of disturbances to the in situ microbial
- community, these changes may be similar to the spectrum of potential micro-environments crustal
- fluid microbes might experience between fluid flow paths or different thermal regimes beneath
- the seafloor (e.g., 5, 46). Samples remained within a 10-15°C range of in situ temperatures during
- the entire sampling and preparation process. A subset of large-scale (1 L) incubations were
- attempted near *in situ* pressures with fluids that were repressurized onboard; however, they
 - formed a cloudy, "rust colored" precipitate and so it was determined the geochemical conditions
- those incubations differed too much from the unpressurized samples to be comparable in this
- study and were not included.
- We compare our results to SIP-NanoSIMS incubations from hydrothermal vent fluids that
- remained pressurized throughout sampling and experimentation (Table S5), but also experienced
- dramatic temperature changes during the collection and incubation preparation process (dropping
- from hydrothermal vent fluid temperatures to bottom water temperatures of ~4°C at times). The
- sediment SIP-NanoSIMS incubations used for comparison (Table S5) also underwent significant
- alteration as isotope labels were added by making sediment slurries that alter the *in situ*
- environment of compacted sediments. Therefore, all SIP-NanoSIMS subsurface sediment or fluid
- incubations have had to make some alterations from in situ conditions for the practicalities of
- undertaking these difficult experiments, and as such, results from any of these systems should be
- interpreted as potential rates of activity rather than direct field measurements.
- Finally, while oxygen was not monitored during the incubations, microcosms should have
- remained oxygenated during the full length of all incubations. A separate study of oxygen from
- bottled North Pond fluids collected in 2017 showed almost no change (<4 µmol/L variation) in
- concentration (~300 μmol/L) after 553 days of incubation across sampling horizons (5). Finally,
- the amount of organic carbon provided (<5 μM) was much lower than in situ oxygen
- concentrations (>100 µM), and thus should not be enough to stoichiometrically deplete oxygen
- 364 during the incubation.

Cell enumeration

- For in situ cell counts, fluids were preserved for cell counts in labeled scintillation vials, 2 x 18 ml
- sample, with 1.8 ml 37% formaldehyde. Vials were mixed via shaking after adding fixative,
- sealed with electrical tape, and stored at 4°C. Cells were quantified using DAPI DNA stain and
- 370 100X objective on an epifluorescence microscope (Table 1).
- For incubation cell counts, incubations were ended by removing ~2 mL of the fluid, followed by
- the addition of 1.9 ml 40% paraformaldehyde (PFA). Each bottle was shaken gently and stored at
- 4°C until filtration on shore. Cell density was quantified in each incubation using the DAPI DNA
 - stain on a 0.22 µm polycarbonate membrane (MilliporeSigma) and visualized under 100X
- objective on an epifluorescence microscope (47). Replicates were pooled for a given incubation
- condition, with 3 mL from each replicate filtered together for a total of 10 ml.
- 378 Diatom lysate
- For the diatom lysate amendment, *Thalassiosira* sp. were grown to a density of 10⁶ ml⁻¹ in f/2
- Medium with 8.82 x 10⁻⁴ M ¹⁵N Sodium Nitrate (100% of added nitrate) and of 1 M ¹³C Sodium
 - Bicarbonate (50% of added bicarbonate). All isotopes were from Cambridge Isotopes
- (Tewksbury, MA, USA). The diatom culture was then concentrated 100x via centrifugation,
- processed with 3 freeze thaw cycles to lyse the cells, and 200 µl of this concentrated lysate was

added to each diatom lysate amended microcosm. Assuming no loss during concentration steps, this would be the equivalent of the lysed complex organics of 10^5 diatoms ml⁻¹ incubation or 4 μ M total C (10^{-12} molC/diatom) and 2 μ M 13 C Diatom. Using the Redfield ratio, this would yield 0.6 μ M nitrogen for that amount of carbon. Therefore, we estimated 4 μ M diatom concentrate carbon was equivalent to 2 μ M 13 C and 4 μ M 15 N was added to each diatom lysate condition.

DIC measurement

Whole fluids were sampled for DIC measurement by peristaltic pump transfer from Tedlar fluid bags through acid-cleaned Masterflex Biopharm tubing into 100 mL glass bottles sealed with ground glass stoppers and Apiezon M grease. Bottles and tubing were pre-cleaned with 10% HCl and glass bottles and stoppers were subsequently cleaned of organic carbon residues by muffling at 450°C. DIC samples were preserved with 20 μL of saturated HgCl2 solution and stored at room temperature in the dark until analysis. DIC concentrations were measured on an AS-C3 analyzer (Apollo Scitech, Newark, DE, United States) after acidification with phosphoric acid and quantification as CO2 by a Li-COR infrared gas analyzer. DIC concentrations were calibrated against certified reference material produced by A.G. Dickson (Scripps Institution of Oceanography, San Diego, CA, United States), and each sample was measured in duplicate with repeat concentrations within 0.1% and measurement uncertainty of 2 μ mol/kg. Overall uncertainty is likely somewhat higher due to fluid handling during recovery and transfer to sample bottles. We assign a conservative estimate of $\pm 5~\mu$ mol/kg for DIC concentrations.

DOC measurement

Whole fluids were sampled for DOC measurement similarly to DIC samples and collected in 1000 mL amber glass bottles sealed with PTFE-lined lids. Concentrations from unfiltered samples are presented here. DOC concentrations were measured at the National Ocean Sciences Accelerator Mass Spectrometry (NOSAMS) facility as the CO_2 yield after ultraviolet photo-oxidation of total DOC. CO_2 concentrations were determined by manometric quantification with uncertainty of $\pm 2~\mu M$. DOC concentrations reported here for subsurface fluids and bottom water are similar to those reported previously (6).

Elemental analysis and isotope mass balance calculations

Pre-combusted 1.0 µm AP15 glass fiber filters (MilliporeSigma) were washed 3X with artificial seawater and then dried in a 50°C oven overnight in individual sterile petri plates. Filters were analyzed at the Marine Biological Laboratory Stable Isotope Laboratory for δ^{15} N and δ^{13} C using a Europa 20-20 continuous-flow isotope ratio mass spectrometer interfaced with a Europa ANCA-SL elemental analyzer (Sercon Ltd., Cheshire, UK). The analytical precision based on replicate analyses of isotopically homogeneous international standards was \pm -0.1 \% for both δ^{15} N and δ^{13} C measurements, and about 1% relative to the %N and %C. While δ^{15} N was measured. concentrations were too low to accurately quantify. ¹³C-carbon incorporation was calculated for 2 day and 6 day incubations by determination of the total particulate C with a background correction using blank filters (combusted and washed with artificial seawater only). Across all runs, blank filters had an average C concentration of 0.48 µmol C with a standard deviation of 0.11 µmol. The average value plus one standard deviation for the blank filters measured on each run was chosen as the conservative estimate of total background C (0.65 µmol C to 0.58 µmol C across runs; Table S1). We then solved for the total moles of ¹³C that was incorporated into biomass (n_{label}) from the labeled substrate using the estimated ¹³C fractional abundances of the isotope labels used (f_{label}) and average ¹³C fractional abundance of from filters where no C or N label was added that had greater than 14 µg C (f_{initial}; 0.0185; Table S2). This resulted in the following equation: $[n_{\text{final}}(f_{\text{initial}}-f_{\text{final}})]/[f_{\text{initial}}-f_{\text{label}}] = n_{\text{label}}$, where $n_{\text{final}} = n_{\text{label}} + n_{\text{initial}}$ and initial refers to the initial conditions of the experiment, final the final conditions, and label the isotope

Science Advances Manuscript Template Page 9 of 37

label incorporated into biomass. The resulting moles of 13 C ($n_{\rm final}$) was then divided by the total volume filtered (144 ml per filter from all replicate incubations) and the length of the respective incubation. Diatom samples were not included in elemental analysis since remaining 13 C/ 15 N labeled diatom particles were included on the filters. Samples were listed as below detection when either 1) the total C was below the blank filter estimate or 2) the 13 C fractional abundance was below the estimate for unlabeled biomass, either of which would result in a negative value for $n_{\rm label}$.

Using 2017 fluid geochemistry, in situ ¹³C-DIC was 8.4 % ¹³C. However, taking into account the dilution of the in situ DIC concentration from the addition of 5 ml ²H₂O, the atom % ¹³C would be between 9 and 10 atom% ¹³C. Therefore, an estimate of 10 atom % ¹³C was used for the ¹³C fractional abundance for DIC amended incubations, which would err on the side of underestimating rate of uptake. As there were no measurements of acetate, methylamine, or diatom lysate, we used 1.5 µM in situ concentration as an estimate for ¹³C isotope dilution calculations based on an estimated 15% of low molecular weight DOM (~10 μM). This yielded an estimated 50 atom % ¹³C acetate, 73 atom % ¹³C methylamine, and 57 atom % ¹³C diatom lysate. Ammonium concentrations were all below detection from 2017, but utilizing 2014 data they ranged from <0.02 to $0.15 \mu M$, which would yield enrichment ranging from 6.3 to 33 atom %. However, enrichment as high as 60 atom % was observed in ammonium incubations (Figure S4), suggesting ammonium concentrations may have been even lower in 2017, possibly as low as 0.0055 µM or 5.5 nM (64.5 atom % enrichment). We also used 5.5 nM for the remaining organic nitrogen concentrations, yielding 99.9 atom % ¹⁵N methylamine and 99.1 atom % ¹⁵N diatom lysate. Final estimates for each amendment are in Table S3. These estimates were rounded to 1 significant figure given the combined uncertainties of measurement errors and estimation of in situ concentrations of C and N compounds. Estimated values were below maximal fractional abundance value of ¹³C measured for each condition, where DIC amended incubations do not exceed 0.1 f¹³C and the remaining incubations do not exceed 0.5 f¹³C or f¹⁵N.

For the NanoSIMS derived average rates plotting with bulk EA data, average single cell measurements were multiplied by the cell density for each incubation. Cell counts and NanoSIMS were performed on 0.22 µm PES filters, but elemental analysis was carried out on 1.0 µm GFF filters, therefore some biomass which was analyzed by the first two techniques may have been missed by the elemental analysis. PFA fixation has also been shown to under-estimate biomass incorporation rates (~10% loss in carbon; (48). Elemental analysis therefore likely represents a lower estimate of the total incubation biomass production.

NanoSIMS analysis and single cell rate calculations

A subset of 12 hr U1383C Shallow and Deep incubations were analyzed via Nanoscale secondary ion mass spectrometry (NanoSIMS). 12 hour incubations were selected for minimal incubation time and Shallow and Deep as crustal fluid endmembers. For this analysis, the remaining sample after cell counts was pooled from each replicate (~144 mL), filtered (0.22 μm polycarbonate membrane; MilliporeSigma), washed with artificial seawater, dehydrated with ethanol, and gold coated (10 nm) prior to analysis. Masses 1 (¹H), 2 (²H), 24 (¹²C₂), 25 (¹³C¹²C), 26 (¹⁴N¹²C), and 27 (¹⁵N¹²C) were collected for all samples along with the secondary electrons using a NanoSIMS-50L (Cameca, Gennevilliers Cedex, France) at the Caltech Microanalysis Center. A focused primary Cs⁺ beam was used for data collection after pre-sputtering to stabilize ion counts. Three frames of 512 x 512 px were collected for each sample.

The data were processed using Look@NanoSIMS software (49). Individual ion image frames were merged and aligned using the ¹²C¹⁴N ion image to correct for drift during acquisition. Cell-based regions of interest (ROIs) were determined by "interactive thresholding" with the ¹²C¹⁴N ion and ²H images. Final ion images and counts per ROI were calculated by summation of ion counts for each pixel over all scans. For NanoSIMS isotope incorporation plots, only ROIs with

Science Advances Manuscript Template Page 10 of 37

counts greater than 2x the Poisson error of the NanoSIMS measurement were displayed. ROIs were also visually inspected to look for potential charging effects or edge effects that may affect isotopic measurements. A one-point correction was also applied to the C and N isotope values based on methods in (12) using EA measurements of the polycarbonate filter (Table S1).

Single cell incorporation rates were calculated utilizing the same method as the bulk rates except amount of C and N per cell was calculated using ROI size information from NanoSIMS images. First, cell volume was estimated based on the area of an ROI (Figure S5). Then per cell volume was converted to fg C and fg N per cell the formulas from (50). For comparison, estimates of 86 fg C and 20 fg N per cell have been used to represent biomass estimates from subsurface sedimentary environments (11). The range of C (21 - 443 fg cell⁻¹) and N (6 - 76 fg cell⁻¹) across all ROIs is plotted in Figure S6. The largest ROIs consist of aggregates of cells that could not be visually divided. Data analysis and display as violin plots or boxplots were done using R (51) with the "ggplot2" (44), "dplyr" (52), "gridExtra" (53), and "RColorBrewer" (54) packages. Cell counts for each incubation were used to convert from fmol/cell/day to pmol/ml/day (Table 3).

Global Rate Calculations

Global rate calculations were computed by multiplying the 12 hr single-cell NanoSIMS rates by the in situ cell concentration (3,700 cells/ml for both U1383C Shallow and Deep) to get fmol per ml per day. This rate was then converted to mol per cubic meter per year by estimating the integral from 1 to 10 of a function for crustal volume versus age (55). This estimate for young (<10 Ma) crust that could be occupied by the suboceanic biosphere (1×10^{17} m³) was then multiplied by an estimated crustal porosity of 1% (56), resulting in an estimated habitable pore volume for young ridge flank crust of 10^{15} m³. This estimated crustal fluid volume was multiplied by the single cell rates to calculate mol per year production (Table 3).

References

- 1. A. Fisher, C. G. Wheat, Seamounts as Conduits for Massive Fluid, Heat, and Solute Fluxes on Ridge Flanks. *Oceanog.* **23**, 74–87 (2010).
- 2. C. G. Wheat, A. T. Fisher, J. McManus, S. M. Hulme, B. N. Orcutt, Cool seafloor hydrothermal springs reveal global geochemical fluxes. *Earth and Planetary Science Letters*. **476**, 179–188 (2017).
 - 3. H. P. Johnson, M. J. Pruis, Fluxes of fluid and heat from the oceanic crustal reservoir. *Earth and Planetary Science Letters*. **216**, 565–574 (2003).
- M. G. Langseth, K. Becker, R. P. V. Herzen, P. Schultheiss, Heat and fluid flux through sediment on the
 western flank of the Mid-Atlantic Ridge: A hydrogeological study of North Pond. *Geophysical Research Letters.* 19, 517–520 (1992).
- 521 5. C. G. Wheat, K. Becker, H. Villinger, B. N. Orcutt, T. Fournier, A. Hartwell, C. Paul, *Geochemistry, Geophysics, Geosystems.* **21**, e2019GC008804 (2020).
- 523 6. N. Jiao, G. J. Herndl, D. A. Hansell, R. Benner, G. Kattner, S. W. Wilhelm, D. L. Kirchman, M. G. 524 Weinbauer, T. Luo, F. Chen, F. Azam, Microbial production of recalcitrant dissolved organic matter: 525 long-term carbon storage in the global ocean. *Nature Reviews Microbiology*. **8**, 593–599 (2010).
- 7. D. A. Hansell, C. A. Carlson, Biogeochemistry of Marine Dissolved Organic Matter (Elsevier, 2015).

Science Advances Manuscript Template Page 11 of 37

- 527 8. J. L. Meyer, U. Jaekel, B. J. Tully, B. T. Glazer, C. G. Wheat, H.-T. Lin, C.-C. Hsieh, J. P. Cowen, S. M. Hulme, P. R. Girguis, J. A. Huber, A distinct and active bacterial community in cold oxygenated fluids circulating beneath the western flank of the Mid-Atlantic ridge. *Scientific Reports*. **6**, 22541 (2016).
- S. R. Shah Walter, U. Jaekel, H. Osterholz, A. T. Fisher, J. A. Huber, A. Pearson, T. Dittmar, P. R.
 Girguis, Microbial decomposition of marine dissolved organic matter in cool oceanic crust. *Nature Geoscience*. 11, 334 (2018).
- 533 10. S. D'Hondt, F. Inagaki, B. Orcutt, K.-U. Hinrichs, IODP Advances in the Understanding of Subseafloor Life. *Oceanog.* **32**, 198–207 (2019).
- 535 11. Y. Morono, T. Terada, M. Nishizawa, M. Ito, F. Hillion, N. Takahata, Y. Sano, F. Inagaki, Carbon and nitrogen assimilation in deep subseafloor microbial cells. *Proceedings of the National Academy of Sciences of the United States of America.* **108**, 18295–300 (2011).
- E. Trembath-Reichert, Y. Morono, A. Ijiri, T. Hoshino, K. S. Dawson, F. Inagaki, V. J. Orphan, Methyl compound use and slow growth characterize microbial life in 2-km-deep subseafloor coal and shale
 beds. *Proceedings of the National Academy of Sciences of the United States of America*. 114, E9206–
 E9215 (2017).
- 13. Y. Morono, M. Ito, T. Hoshino, T. Terada, T. Hori, M. Ikehara, S. D'Hondt, F. Inagaki, Aerobic microbial life persists in oxic marine sediment as old as 101.5 million years. *Nature Communications*. **11**, 3626 (2020).
- 545 14. J. McNichol, H. Stryhanyuk, S. P. Sylva, F. Thomas, N. Musat, J. S. Seewald, S. M. Sievert, Primary 546 productivity below the seafloor at deep-sea hot springs. *Proceedings of the National Academy of* 547 *Sciences of the United States of America*. **115**, 6756–6761 (2018).
- M. Winkel, P. Pjevac, M. Kleiner, S. Littmann, A. Meyerdierks, R. Amann, M. Mußmann, Identification
 and activity of acetate-assimilating bacteria in diffuse fluids venting from two deep-sea
 hydrothermal systems. *FEMS Microbiol Ecol.* 90, 731–746 (2014).
- 551 16. E. Trembath-Reichert, D. A. Butterfield, J. A. Huber, Active subseafloor microbial communities from Mariana back-arc venting fluids share metabolic strategies across different thermal niches and taxa.

 553 The ISME Journal. 13, 2264–2279 (2019).
- 17. A. N. Price, A. T. Fisher, T. S. Weathers, C. W. Gable, P. H. Stauffer, Two- and Three-Dimensional
 Numerical Simulations of Coupled Fluid and Heat Flow Processes Beneath a Marine Sediment Pond.
 AGU Fall Meeting Abstracts. 33 (2019).
- 18. J. P. Cowen, D. A. Copson, J. Jolly, C.-C. Hsieh, H.-T. Lin, B. T. Glazer, C. G. Wheat, Advanced instrument system for real-time and time-series microbial geochemical sampling of the deep (basaltic) crustal biosphere. *Deep Sea Research Part I: Oceanographic Research Papers*. **61**, 43–56 (2012).
- 19. B. J. Tully, C. G. Wheat, B. T. Glazer, J. A. Huber, A dynamic microbial community with high functional redundancy inhabits the cold, oxic subseafloor aquifer. *The ISME Journal.* **12**, 1–16 (2018).
- 20. B. N. Orcutt, T. D'Angelo, C. G. Wheat, E. Trembath-Reichert, Microbe-mineral biogeography from
 multi-year incubations in oceanic crust at North Pond, Mid-Atlantic Ridge. *Environmental Microbiology*. (2021), doi:https://doi.org/10.1111/1462-2920.15366.

Science Advances Manuscript Template Page 12 of 37

- 566 21. S. P. Jungbluth, J. Grote, H.-T. Lin, J. P. Cowen, M. S. Rappé, Microbial diversity within basement fluids of the sediment-buried Juan de Fuca Ridge flank. *The ISME Journal*. **7**, 161–172 (2013).
- P. Hirsch, E. Rades-Rohkohl, Some Special Problems in the Determination of Viable Counts of
 Groundwater Microorganisms. *Microbial Ecology*. 16, 99–113 (1988).
- 570 23. S. H. Kopf, S. E. McGlynn, A. Green-Saxena, Y. Guan, D. K. Newman, V. J. Orphan, Heavy water and 571 15N labelling with NanoSIMS analysis reveals growth rate-dependent metabolic heterogeneity in 572 chemostats. *Environmental Microbiology*. **17**, 2542–2556 (2015).
- T. Reinthaler, H. M. van Aken, G. J. Herndl, Major contribution of autotrophy to microbial carbon cycling in the deep North Atlantic's interior. *Deep Sea Research Part II: Topical Studies in Oceanography.* 57, 1572–1580 (2010).
- 576 25. B. N. Orcutt, J. B. Sylvan, D. R. Rogers, J. Delaney, R. W. Lee, P. R. Girguis, Carbon fixation by basalt-577 hosted microbial communities. *Front Microbiol.* **6** (2015), doi:10.3389/fmicb.2015.00904.
- 578 26. X. Zhang, X. Feng, F. Wang, Diversity and Metabolic Potentials of Subsurface Crustal Microorganisms 579 from the Western Flank of the Mid-Atlantic Ridge. *Frontiers in microbiology*. **7**, 363 (2016).
- 580 27. W. Bach, K. J. Edwards, Iron and sulfide oxidation within the basaltic ocean crust: implications for chemolithoautotrophic microbial biomass production. *Geochimica et Cosmochimica Acta*. **67**, 3871–3887 (2003).
- 583 28. L. M. Seyler, E. Trembath-Reichert, B. J. Tully, J. A. Huber, Time-series transcriptomics from cold, oxic 584 subseafloor crustal fluids reveals a motile, mixotrophic microbial community. *The ISME Journal*, 1– 585 15 (2020).
- 586 29. Y. Suzuki, S. Yamashita, M. Kouduka, Y. Ao, H. Mukai, S. Mitsunobu, H. Kagi, S. D'Hondt, F. Inagaki, Y. Morono, T. Hoshino, N. Tomioka, M. Ito, Deep microbial proliferation at the basalt interface in 33.5–104 million-year-old oceanic crust. *Communications Biology*. **3**, 1–9 (2020).
- 30. O. U. Mason, T. Nakagawa, M. Rosner, J. D. Van Nostrand, J. Zhou, A. Maruyama, M. R. Fisk, S. J.
 Giovannoni, First Investigation of the Microbiology of the Deepest Layer of Ocean Crust. *PLoS One*.
 5 (2010), doi:10.1371/journal.pone.0015399.
- J. Li, P. Mara, F. Schubotz, J. B. Sylvan, G. Burgaud, F. Klein, D. Beaudoin, S. Y. Wee, H. J. B. Dick, S.
 Lott, R. Cox, L. A. E. Meyer, M. Quémener, D. K. Blackman, V. P. Edgcomb, Recycling and metabolic flexibility dictate life in the lower oceanic crust. *Nature*. 579, 250–255 (2020).
- 595 32. P. J. Large, D. Peel, J. R. Quayle, Microbial growth on C1 compounds. 2. Synthesis of cell constituents 596 by methanol- and formate-grown Pseudomonas AM1, and methanol-grown Hyphomicrobium 597 vulgare. *Biochem J.* **81**, 470–480 (1961).
- 33. R. Peyraud, K. Schneider, P. Kiefer, S. Massou, J. A. Vorholt, J.-C. Portais, Genome-scale
 reconstruction and system level investigation of the metabolic network of Methylobacterium
 extorquensAM1. BMC Systems Biology. 5, 189 (2011).
- 34. J. M. Arrieta, E. Mayol, R. L. Hansman, G. J. Herndl, T. Dittmar, C. M. Duarte, Dilution limits dissolved organic carbon utilization in the deep ocean. *Science*. **348**, 331–333 (2015).

Science Advances Manuscript Template Page 13 of 37

- 35. A. Schwedt, M. Seidel, T. Dittmar, M. Simon, V. Bondarev, S. Romano, G. Lavik, H. N. Schulz-Vogt,
 Substrate Use of Pseudovibrio sp. Growing in Ultra-Oligotrophic Seawater. *PLOS ONE*. 10, e0121675
 (2015).
- 36. B. Widner, C. A. Fuchsman, B. X. Chang, G. Rocap, M. R. Mulholland, Utilization of urea and cyanate
 in waters overlying and within the eastern tropical north Pacific oxygen deficient zone. *FEMS Microbiol Ecol.* 94 (2018), doi:10.1093/femsec/fiy138.
- 37. J. P. Cowen, D. A. Copson, J. H. Jolly, C.-C. Hsieh, H.-T. Lin, B. T. Glazer, C. G. Wheat. Advanced
 instrument system for real-time and time-series microbial geochemical sampling of the deep
 (basaltic) crustal biosphere. 61, 43-56 (2012).
- 38. A. Apprill, S. McNally, R. Parsons, L. Weber, Minor revision to V4 region SSU rRNA 806R gene primer greatly increases detection of SAR11 bacterioplankton. *Aquatic Microbial Ecology*. **75**, 129–137 (2015).
- 39. J. G. Caporaso, C. L. Lauber, W. A. Walters, D. Berg-Lyons, J. Huntley, N. Fierer, S. M. Owens, J. Betley,
 L. Fraser, M. Bauer, N. Gormley, J. A. Gilbert, G. Smith, R. Knight, Ultra-high-throughput microbial
 community analysis on the Illumina HiSeq and MiSeq platforms. *The ISME Journal*. 6, 1621–1624
 (2012).
- 40. J. G. Caporaso, C. L. Lauber, W. A. Walters, D. Berg-Lyons, C. A. Lozupone, P. J. Turnbaugh, N. Fierer,
 R. Knight, Global patterns of 16S rRNA diversity at a depth of millions of sequences per sample.
 PNAS. 108, 4516–4522 (2011).
- 41. A. E. Parada, D. M. Needham, J. A. Fuhrman, Every base matters: assessing small subunit rRNA
 primers for marine microbiomes with mock communities, time series and global field samples.
 Environmental Microbiology. 18, 1403–1414 (2016).
- 42. C. Quast, E. Pruesse, P. Yilmaz, J. Gerken, T. Schweer, P. Yarza, J. Peplies, F. O. Glöckner, The SILVA
 ribosomal RNA gene database project: improved data processing and web-based tools. *Nucleic Acids Research.* 41, D590–D596 (2012).
- 43. J. Oksanen, F. G. Blanchet, M. Friendly, R. Kindt, P. Legendre, D. McGlinn, P. R. Minchin, R. B. O'Hara,
 629 G. L. Simpson, P. Solymos, M. H. H. Stevens, E. Szoecs, H. Wagner, *vegan: Community Ecology* 630 *Package* (2017; https://cran.r-project.org/package=vegan).
- 44. H. Wickham, *ggplot2: Elegant Graphics for Data Analysis* (Springer-Verlag New York, 2016; https://ggplot2.tidyverse.org).
- 45. K. Becker, A. Bartetzko, E. E. Davis, Leg 174B synopsis: revisiting Hole 395A for logging and long-term
 634 monitoring of off-axis hydrothermal processes in young oceanic crust. *Proc. ODP, Sci. Results B.* 174,
 635 1–13 (2001).
- 46. A. T. Fisher, Permeability within basaltic oceanic crust. *Reviews of Geophysics*. **36**, 143–182 (1998).
- 47. K. G. Porter, Y. S. Feig, The use of DAPI for identifying and counting aquatic microflora1. *Limnology* and Oceanography. **25**, 943–948 (1980).
- 48. N. Musat, H. Stryhanyuk, P. Bombach, L. Adrian, J.-N. Audinot, H. H. Richnow, The effect of FISH and
 CARD-FISH on the isotopic composition of 13C- and 15N-labeled Pseudomonas putida cells
 measured by nanoSIMS. Systematic and Applied Microbiology. 37, 267–276 (2014).

Science Advances Manuscript Template Page 14 of 37

- 49. L. Polerecky, B. Adam, J. Milucka, N. Musat, T. Vagner, M. M. M. Kuypers, Look@NanoSIMS a tool for the analysis of nanoSIMS data in environmental microbiology. *Environmental Microbiology*. **14**, 1009–1023 (2012).
- 50. A. Khachikyan, J. Milucka, S. Littmann, S. Ahmerkamp, T. Meador, M. Könneke, T. Burg, M. M. M.
 Kuypers, Direct Cell Mass Measurements Expand the Role of Small Microorganisms in Nature. *Appl. Environ. Microbiol.* 85 (2019), doi:10.1128/AEM.00493-19.
- 51. R Core Team, *R: A Language and Environment for Statistical Computing* (R Foundation for Statistical Computing, Vienna, Austria, 2017; https://www.r-project.org/).
- 52. H. Wickham, R. François, L. Henry, K. Müller, RStudio, *dplyr: A Grammar of Data Manipulation* (2020; https://CRAN.R-project.org/package=dplyr).
- 53. B. Auguie, A. Antonov, *gridExtra: Miscellaneous Functions for "Grid" Graphics* (2017; https://CRAN.R-project.org/package=gridExtra).
- 54. E. Neuwirth, *RColorBrewer: ColorBrewer Palettes* (2014; https://CRAN.R-project.org/package=RColorBrewer).
- 55. C. Heberling, R. P. Lowell, L. Liu, M. R. Fisk, Extent of the microbial biosphere in the oceanic crust. *Geochemistry, Geophysics, Geosystems.* **11** (2010), doi:10.1029/2009GC002968.
- 56. B. N. Orcutt, C. G. Wheat, O. Rouxel, S. Hulme, K. J. Edwards, W. Bach, Oxygen consumption rates in
 subseafloor basaltic crust derived from a reaction transport model. *Nature Communications*. 4,
 2539 (2013).

Acknowledgments

- We thank the captain and crew of the R/V Atlantis, the pilots and engineers of the ROV Jason,
 - and B. Orcutt, C. G. Wheat, M. Mullis, K. Yoshimura, O. Nigro, B. Tully, G. Stewart, K. Freel,
- 665 C. Sullivan, and M. Rappé for their assistance in accomplishing the field program. We thank M.
- Otter for analytical assistance and resources for POC isotopic and mass measurements; N.
- Hussain and W.-J. Cai for analytical assistance and resources for bicarbonate measurements; M.
- Johnson for growing and providing the diatom culture; V. Orphan and Y. Guan for access and
- assistance with NanoSIMS analysis; M. Serres, J. Amend, and D. LaRowe for helpful discussions
- 670 regarding these data.

Funding:

661 662

664

- The Gordon and Betty Moore Foundation sponsored most of the observatory components at North
- Pond through grant GBMF1609.
- The National Science Foundation NSF OCE-1745589, OCE-1635208, and OCE-1062006 to
- 676 J.A.H and NSF OCE-1635365 to P.R.G and S.S.W.
- NASA Postdoctoral Fellowship with the NASA Astrobiology Institute to E.T.R
- 678 L'Oréal USA For Women in Science Fellowship to E.T.R.
- Woods Hole Partnership Education Program, sponsored by the Woods Hole Diversity Initiative to
- 680 M.F.O.
- The Center for Dark Energy Biosphere Investigations (C-DEBI OCE-0939564) also supported the
- participation of J.A.H. and P.C. This is C-DEBI contribution number XXX.

684	Author contributions:
685	Conceptualization: ETR, JAH, SSW, PRG
686	Investigation: ETR, MFO, PC, SSW
687	Writing—original draft: ETR, JAH
688	Writing—review & editing: ETR, JAH, SSW, PRG
689	
690	Competing interests: Authors declare that they have no competing interests.
691	
692	Data and materials availability: Raw sequencing data is available through the NCBI Short Read
693	Archive under project number: PRJNA603242. All remaining data are in the main text and
694	supplementary materials.
695	

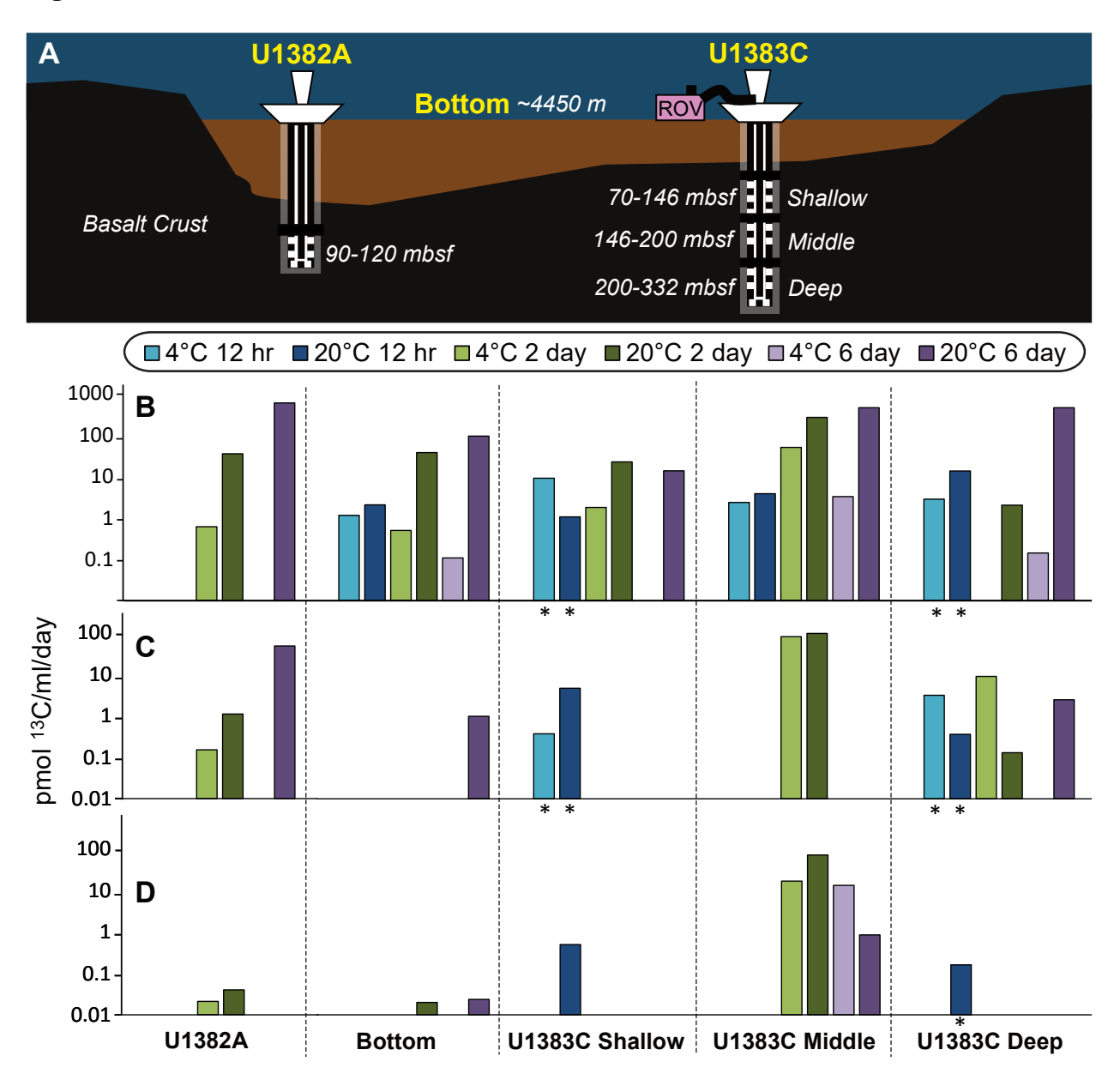


Figure 1. North Pond is located in young, cool crust (8 Ma) with a "sediment pond" roughly 13 km long by 7 km wide and up to 200 m deep. (**A**) Diagram of CORK observatories at North Pond with different sampling locations (U1382A, bottom seawater, and U1383C) and depths in meters below surface (m) or meters below seafloor (mbsf). U1383C is located about 6 km to the NE of U1382A. Bulk ¹³C-carbon isotope incorporation rates calculated from (**B**) ¹³C acetate, (**C**) ¹³C bicarbonate, and (**D**) ¹³C methylamine SIP incubations of each fluid sample for 12 hour, 2 day, and 6 day incubation periods in order shown in (**A**). Asterisk indicates value computed from SIP-NanoSIMS single cell measurements (Table 3) instead of bulk Elemental Analysis. No bar indicates the data are below detection (see methods).

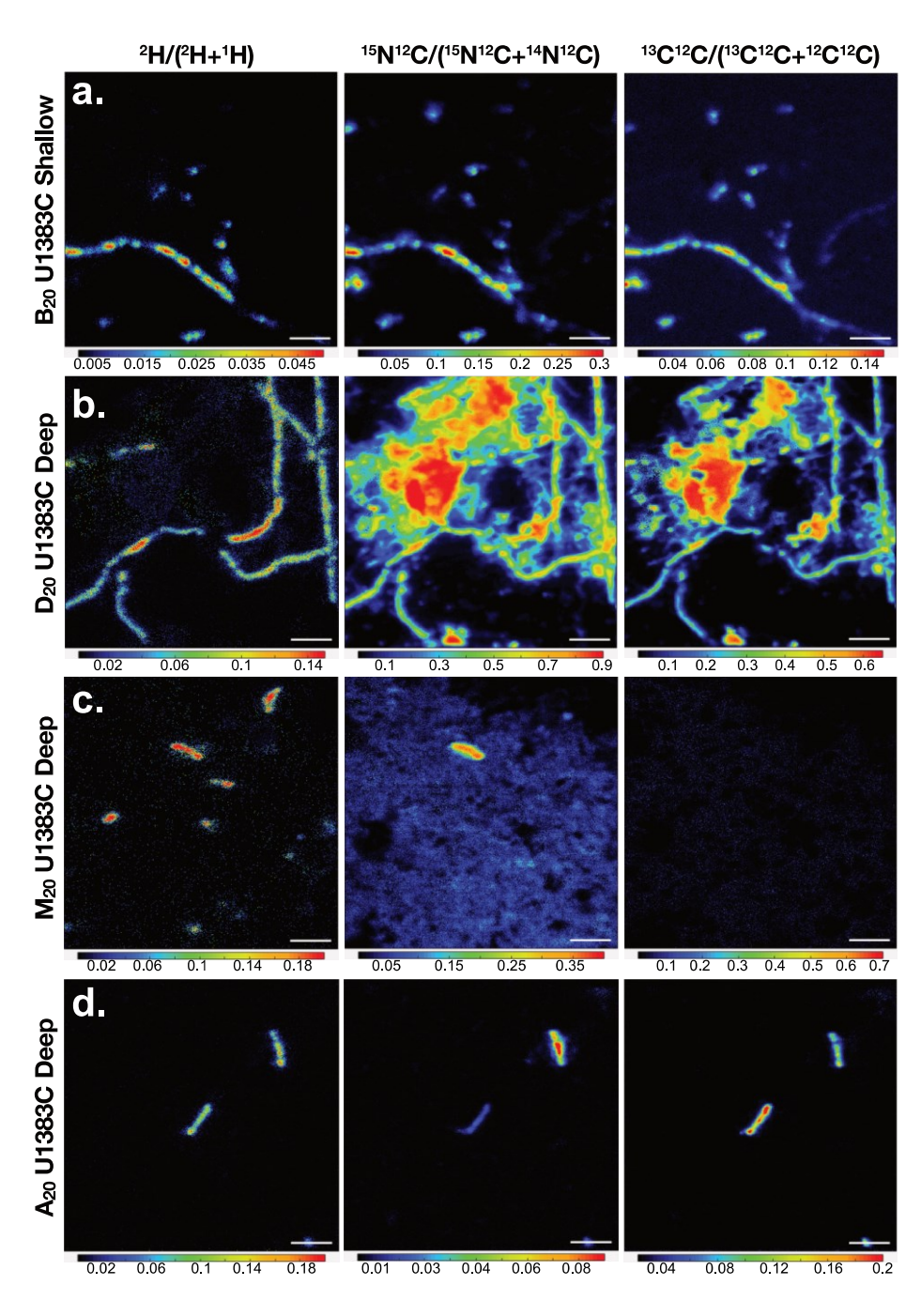


Figure 2. Selected NanoSIMS ratio images for each stable isotope (²H, ¹⁵N, and ¹³C). a) The most active Shallow sample amended with ¹³C-DIC and ¹⁵N-ammonium (B₂₀ U1383C Shallow), b) U1383C Deep ¹³C¹⁵N diatom lysate amendment, where remaining diatom lysate is visible in ¹⁵N and ¹³C images, but ²H uptake is only seen in associated filaments (D₂₀ U1383C Deep), c) ¹³C¹⁵N methylamine uptake in ²H and ¹⁵N without visible ¹³C incorporation (M₂₀ U1383C Deep), and d) and most active Deep sample (A₂₀ U1383C Deep) amended with ¹³C acetate and ¹⁵N ammonium. All incubations were amended with ²H₂O. 3µm scale bar. Ratio range scale differs between samples to show maximum values per image.

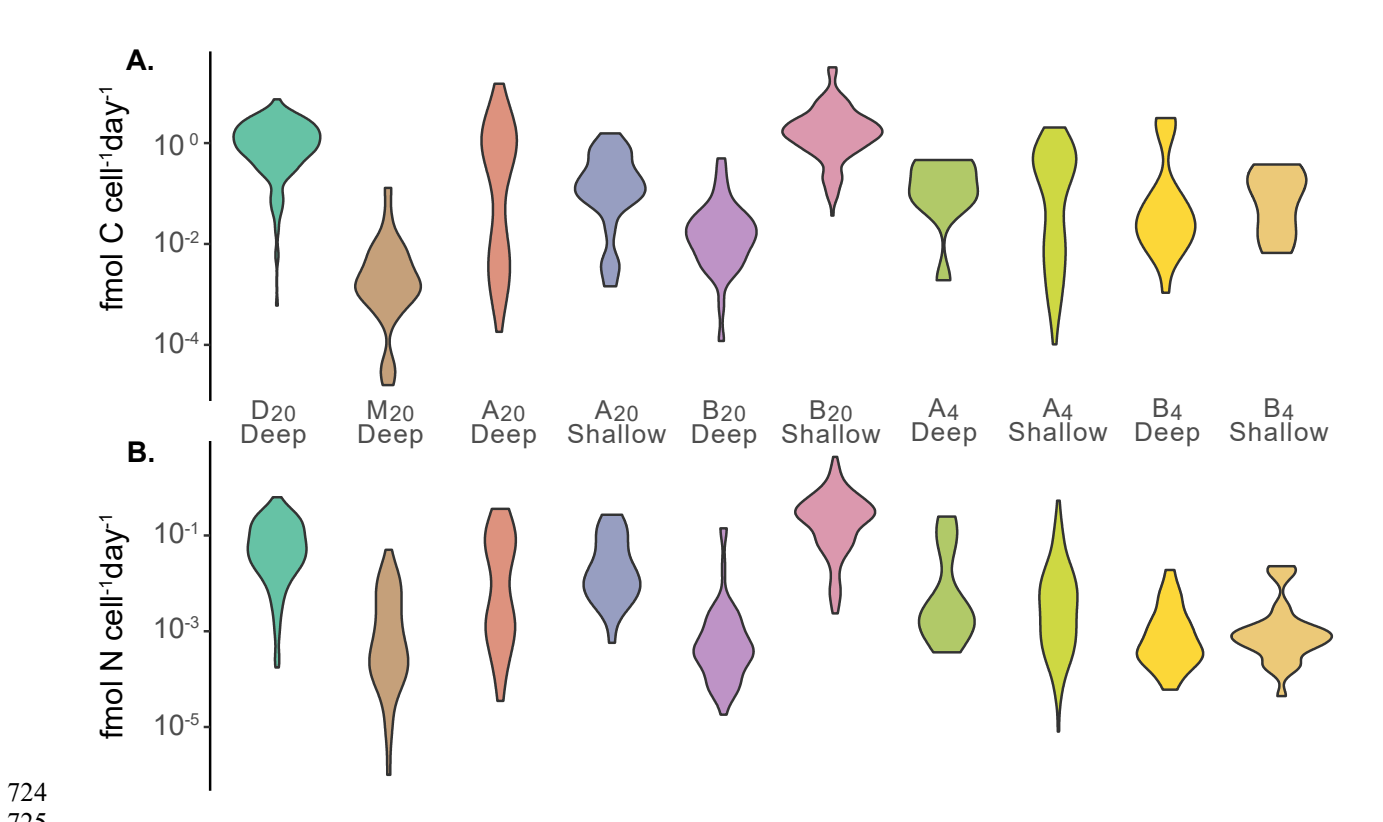


Figure 3. Computed fmol (**A**) C and (**B**) N cell-1day-1 based on single cell isotope incorporation rates from U1383C Shallow and Deep incubations analyzed by NanoSIMS. Plotted as kernel density distribution of the data with true values overlain.

Science Advances Manuscript Template Page 19 of 37

Sample	Depth (m)	Cells x10³ ml ⁻¹	± 95% CI	рН	DIC (μmol/kg)	Ο ₂ (μΜ)	Nitrate (µmol/kg)	DOC (µmol/kg)
Bottom Water	4397*	9.0	0.4	7.92	2188	250	21.8	39
U1382A	90 to 210	5.1	0.2	7.91	2164	228	22.3	31
U1383C Shallow	70 to 146	3.7	0.3	8.07	2167	198	22.8	20
U1383C Middle	146 to 200	2.1	0.2	8.13	2189	205	22.9	22
U1383C Deep	200 to 332	3.7	0.3	8.06	2156	173	22.7	22

Table 1. North Pond CORK fluids and bottom water values for cell enumeration, dissolved inorganic carbon (DIC) and dissolved organic carbon (DOC) from 2017 samples collected for this study. Additional geochemistry (Oxygen, nitrate, and pH) reproduced from (5) also collected in 2017. Ammonium concentrations were all below detection (<0.1 umol/kg) from 2017 (5). *Depth in meters below surface, remaining depths are in meters below seafloor (mbsf). bicarbonate concentrations are \pm 5 µmol/kg.

Science Advances Manuscript Template Page 20 of 37

Condition	² H label	¹³ C label	¹⁵ N label	Temp. (°C)
C_{20}	Water	None	None	20
D_{20}	Water	Diatom lysate	Diatom lysate	20
M_{20}	Water	Methylamine	Methylamine	20
A_{20}	Water	Acetate	Ammonium	20
B ₂₀	Water	Bicarbonate	Ammonium	20
C ₄	Water	None	None	4
D ₄	Water	Diatom lysate	Diatom lysate	4
M_4	Water	Methylamine	Methylamine	4
A_4	Water	Acetate	Ammonium	4
B ₄	Water	Bicarbonate	Ammonium	4

Table 2. Experimental conditions of stable isotope probing incubations for the five fluid sources collected at North Pond (bottom water, U1382A, U1383C Shallow, U1383C Middle, and U1383C Deep). All incubations were conducted in triplicate separate bottles for each time point at 12 hours, 2 days, 6 days. Condition identifiers used in figures referenced here, where C is control, D is diatom lysate, M is methylamine, A is acetate, and B is bicarbonate or bicarbonate and the temperature is in subscript.

Science Advances Manuscript Template Page 21 of 37

Cond.	U1383C Fluid	fmol C cell ⁻¹ d ⁻¹	fmol N cell ⁻¹ d ⁻¹	pmol C ml ⁻¹ d ⁻¹	pmol N ml ⁻¹ d ⁻¹	C:N
D ₂₀	Deep	1.3	0.096	86	6.2	14
M ₂₀	Deep	0.0085	0.0087	0.16	0.17	0.98
A ₂₀	Deep	1.15	0.097	15	1.3	12
B ₂₀	Deep	0.042	0.021	0.4	0.17	2.0
A_4	Deep	0.21	0.12	2	1.5	1.7
B ₄	Deep	0.46	0.0029	3	0.020	155
A_{20}	Shallow	0.30	0.054	1.1	0.2	5.5
B ₂₀	Shallow	3.0	0.42	5	0.6	7.0
A_4	Shallow	0.33	0.025	10	0.8	13
B ₄	Shallow	0.13	0.0085	0.4	0.023	16

Table 3. Average per cell and per ml rates of carbon and nitrogen uptake from NanoSIMS data of 12 hour incubations. Incubations conducted nearest in situ temperatures for each fluid source are shaded in gray.

Science Advances Manuscript Template Page 22 of 37

767

768

769770

771

772

773

774775

Fluid	Cond.	mol C year ¹			mol N year ¹ 754			
	Cona.	Avg	Max	Min	Avg	Max	Miss	
	D_{20}	2×10 ¹²	1×10 ¹²	8×10 ⁸	1×10 ¹¹	8×10 ¹¹	2 √16 68 757	
83C ep	M_{20}	1×10 ¹⁰	2×10 ¹¹	2×10 ⁷	1×10 ¹⁰	7×10 ¹⁰	2×7507	
U1383C Deep	A ₂₀	2×10 ¹²	2×10 ¹³	2×10 ⁸	1×10 ¹¹	5×10 ¹¹	5×10 ⁷ 760	
	B ₂₀	6×10 ¹⁰	7×10 ¹¹	2×10 ⁸	3×10 ¹⁰	2×10 ¹⁰	9×760 ⁷	
U1383C Shallow	A ₄	4×10 ¹¹	3×10 ¹²	1×10 ⁸	3×10 ¹⁰	7×10 ¹¹	762 1×10 ⁷ 763	
U13 Sha	B ₄	2×10 ¹¹	5×10 ¹¹	9×10 ⁹	1×10 ¹⁰	3×10 ¹⁰	6×76 0 7 	

Table 4. Estimated average, maximum, and minimum mol of C or N year⁻¹ produced in young (<10 Ma) crustal fluids for incubations conducted nearest in situ temperatures for each fluid. Estimates are based on single cell average, maximum, and minimum carbon and nitrogen isotope incorporation rates from NanoSIMS analysis for U1383C Shallow and Deep samples.

Supplementary Materials

Figs. S1 to S8 Tables S1 to S5 Dataset S1 to S3

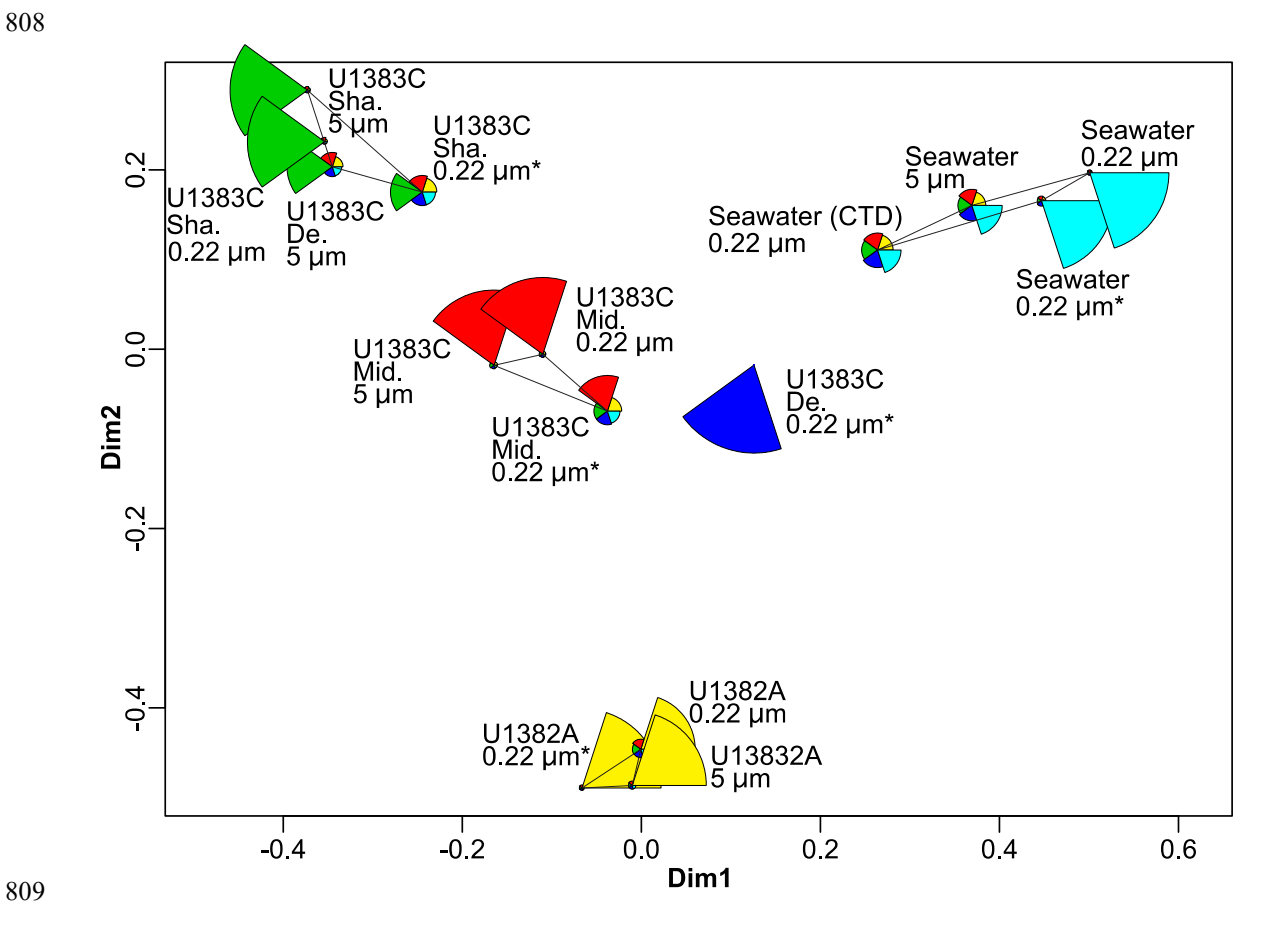


Fig. S1.

CORK and bottom seawater fluids were filtered sequentially through 5 µm and then 0.22 µm filters shipboard, with an additional set of 0.22 µm filters filtered on the seafloor. DNA was extracted from all filters and 16S rRNA gene amplicon libraries were created. Fuzzy logic groupings of the relative abundance of 97% 16S rRNA gene OTUs were generated and indicated that samples grouped by fluid source, with U1382A, bottom seawater, and U1383C Shallow in distinct groups. Wedge size indicates probability of membership. Asterisk indicates samples filtered and preserved on the seafloor, while all others were filtered shipboard. Shallow (Sha.), Middle (Mid.), and Deep (De.) One sample from U1383C Deep grouped with U1383C Shallow samples, while all U1383C Middle samples grouped together. Within the groupings, no distinction between filter size fraction was apparent.

810

811

812

813

814

815

816

817

818

819

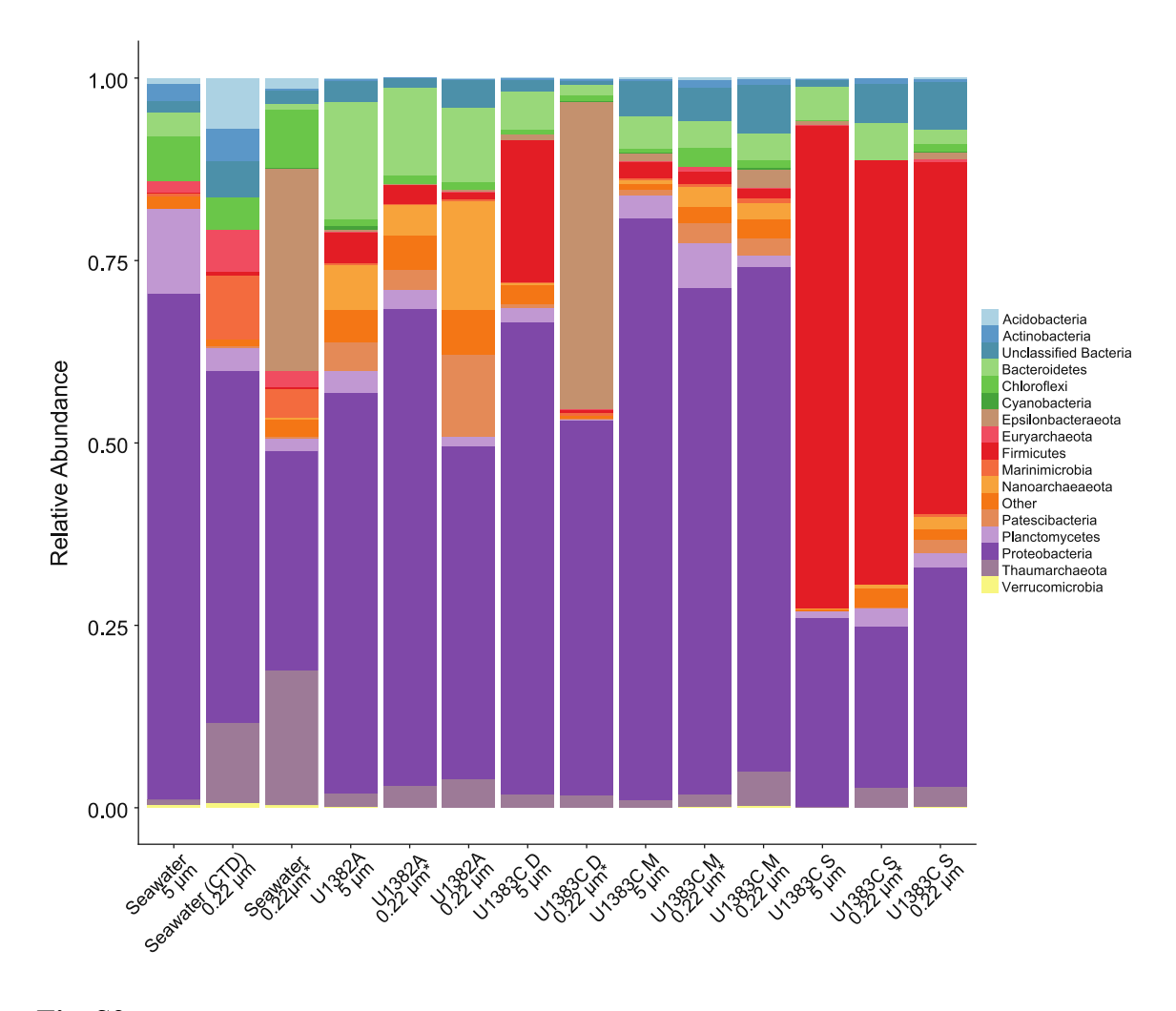


Fig. S2. Relative abundance of 16S rRNA gene sequence 97% OTUs grouped by phylum level taxonomy. All phyla which summed to >10% across all samples are named, the remaining phyla are grouped into Other. Asterisk indicates samples filtered and preserved on the seafloor. Taxonomic analysis of 16S rRNA gene OTUs indicated all samples were dominated by Proteobacteria, with the exception of U1383C Shallow samples, where Firmicutes were the most abundant group (Fig S2). The U1383C Deep sample filtered shipboard through a 5 μ m filter also had a large portion of Firmicutes, whereas the 0.22 μ m in situ filter from U1383C Deep had a large component of Epsilonbacteraeota, similar to the in situ filtered bottom seawater sample (Fig S2).

Science Advances Manuscript Template Page 26 of 37

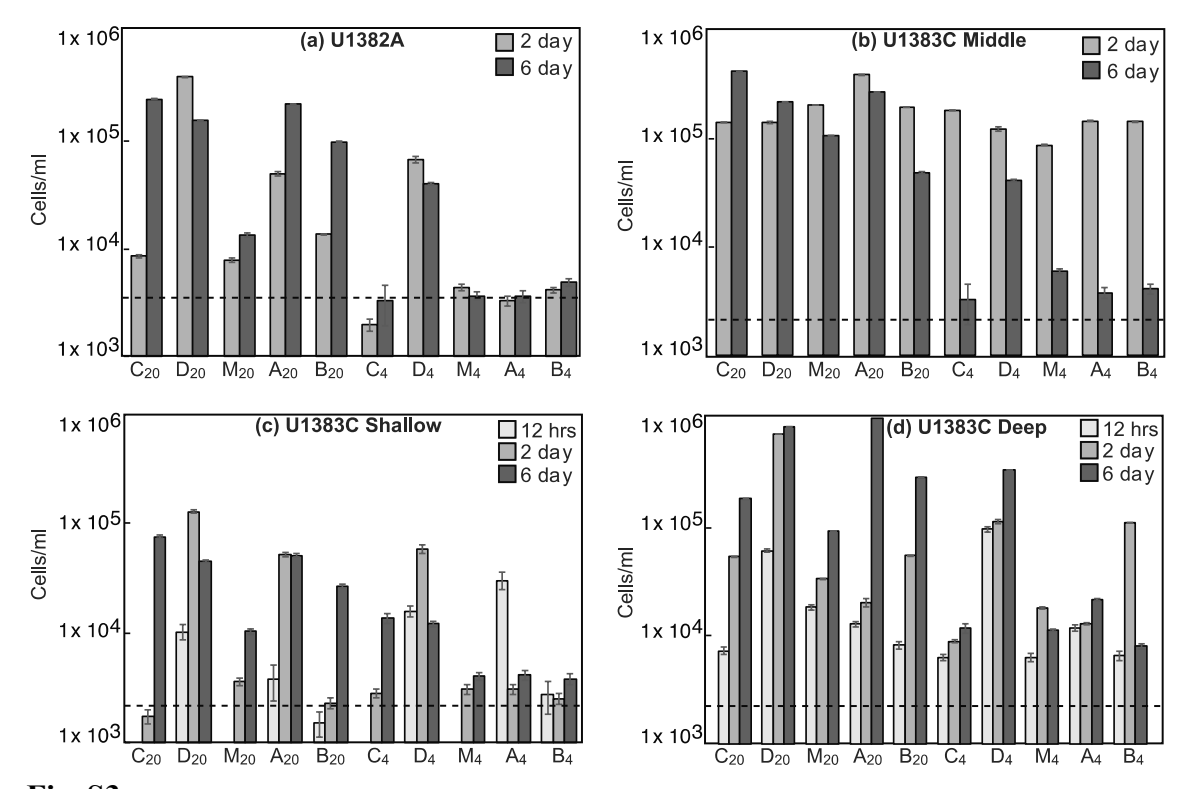


Fig. S3. 12 hour, 2 day, and 6 day SIP incubation cell densities for (a) U1382A, (b) U1383C Middle, (c) U1383C Shallow and (d) U1383C Deep fluids. Cell counts were carried out on all 2 and 6 day crustal fluid incubations, as well as on a subset of the 12 hour incubations with U1383C Shallow and Deep fluids that were used for NanoSIMS analysis. 12 hour incubations were only counted when used for NanoSIMS analysis. Dashed line indicates in situ cell densities from Table 1. Amendments and temperatures are defined in Table 2. No bar indicates analysis was not done. Xaxis labels are provided in Table 2. 95% confidence intervals based on statistical analysis of cells per field of view are presented as error bars.

Science Advances Page 27 of 37 Manuscript Template

836

837

838

839

840

841

842

843 844

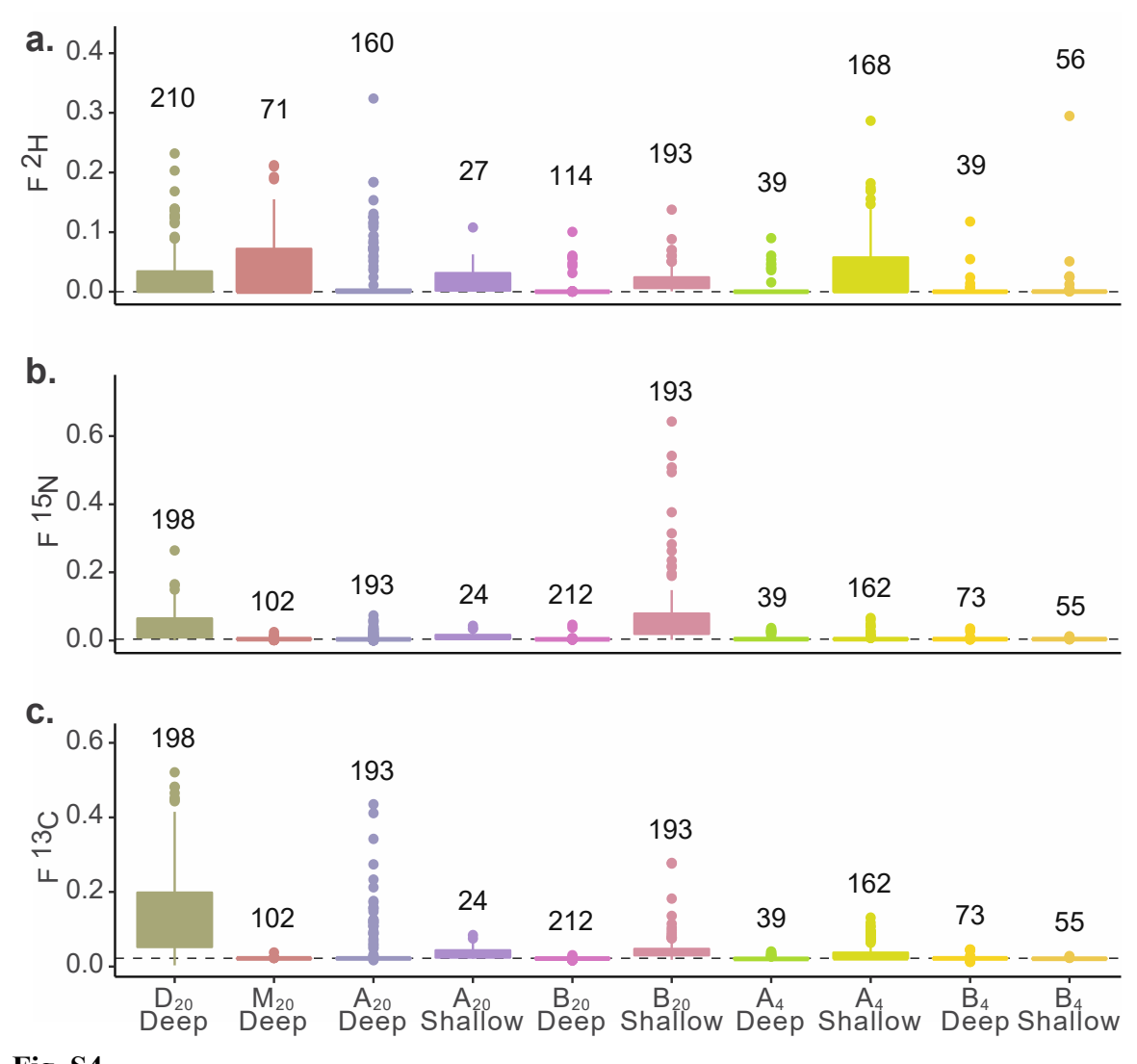


Fig. S4.
Single cell SIP-NanoSIMS measurements of fractional abundance ²H, ¹⁵N, and ¹³C across 12 hour U1383C Shallow and Deep incubations conditions (labeled as per Table 2). Dashed lines indicate natural abundance of each isotope. The number of cells (ROIs) included in the boxplot is provide above each sample. Relative comparison of fractional abundance is only possible across incubations with ²H, since it should have the same elemental enrichment across all incubations, as compared to carbon and nitrogen substrates that vary in final isotopic enrichment (see Methods). Different amendments cannot be compared for ¹⁵N and ¹³C since they had different labeling strengths (e.g. ¹³C acetate label was ~0.5 whereas ¹³C DIC was ~0.1).

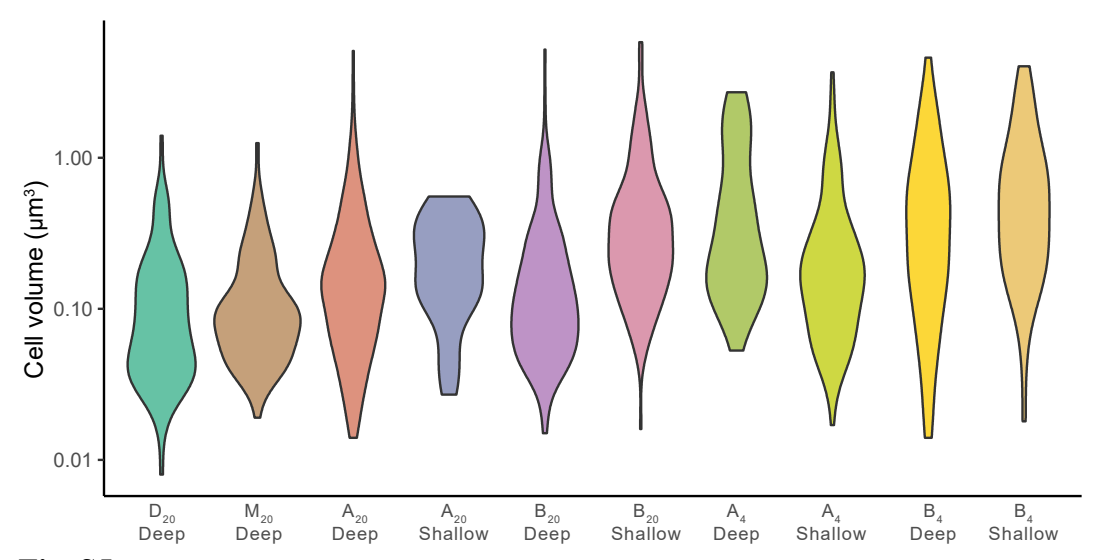


Fig. S5. Estimated volume (μm^3) per ROI (cell) calculated from pixel area of NanoSIMS images for SIP-NanoSIMS incubations.

Science Advances Manuscript Template Page 29 of 37



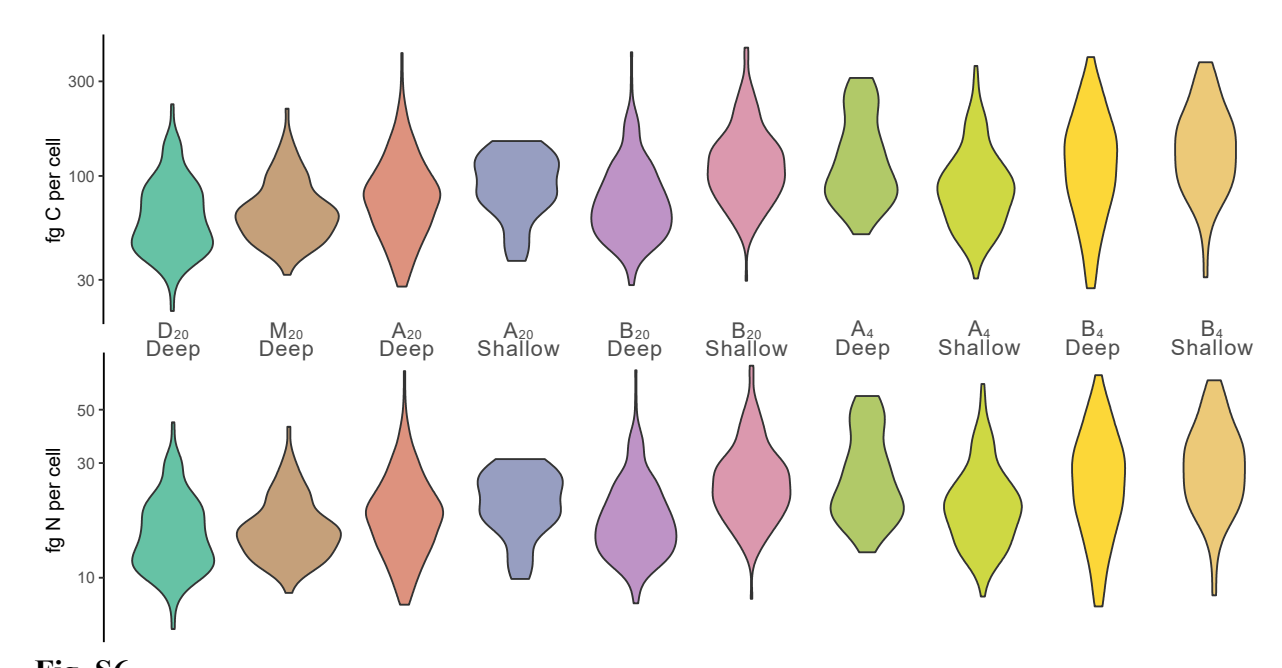


Fig. S6. Fg C and N per ROI (cell) calculated from pixel area of NanoSIMS images for SIP-NanoSIMS incubations.

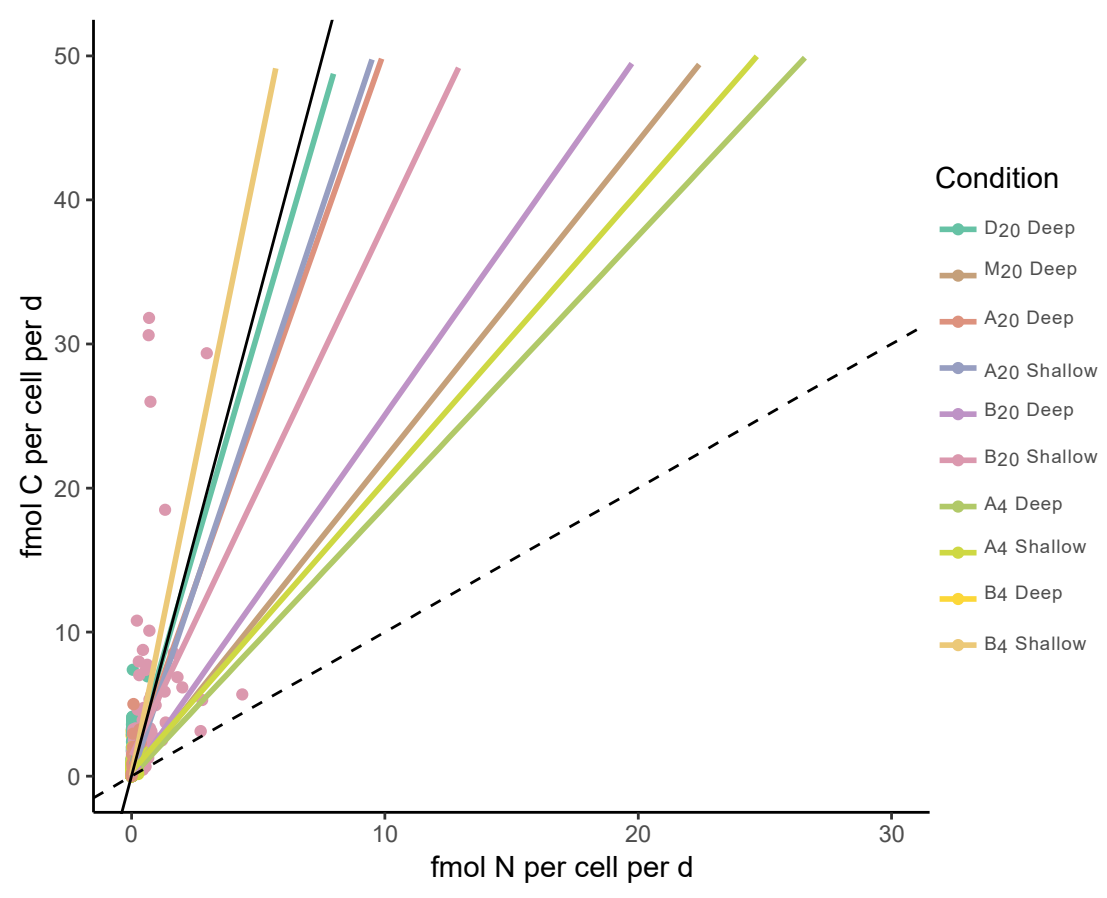


Fig. S7. Linear regression analysis of each SIP-NanoSIMS incubation condition with Redfield (106:16; solid black line) and 1:1 lines for comparison (dashed black line). Sample B4 Deep had a negative regression, likely due to very low N uptake rates, (C:N of 155, Table 3) and is not plotted here.

Page 31 of 37

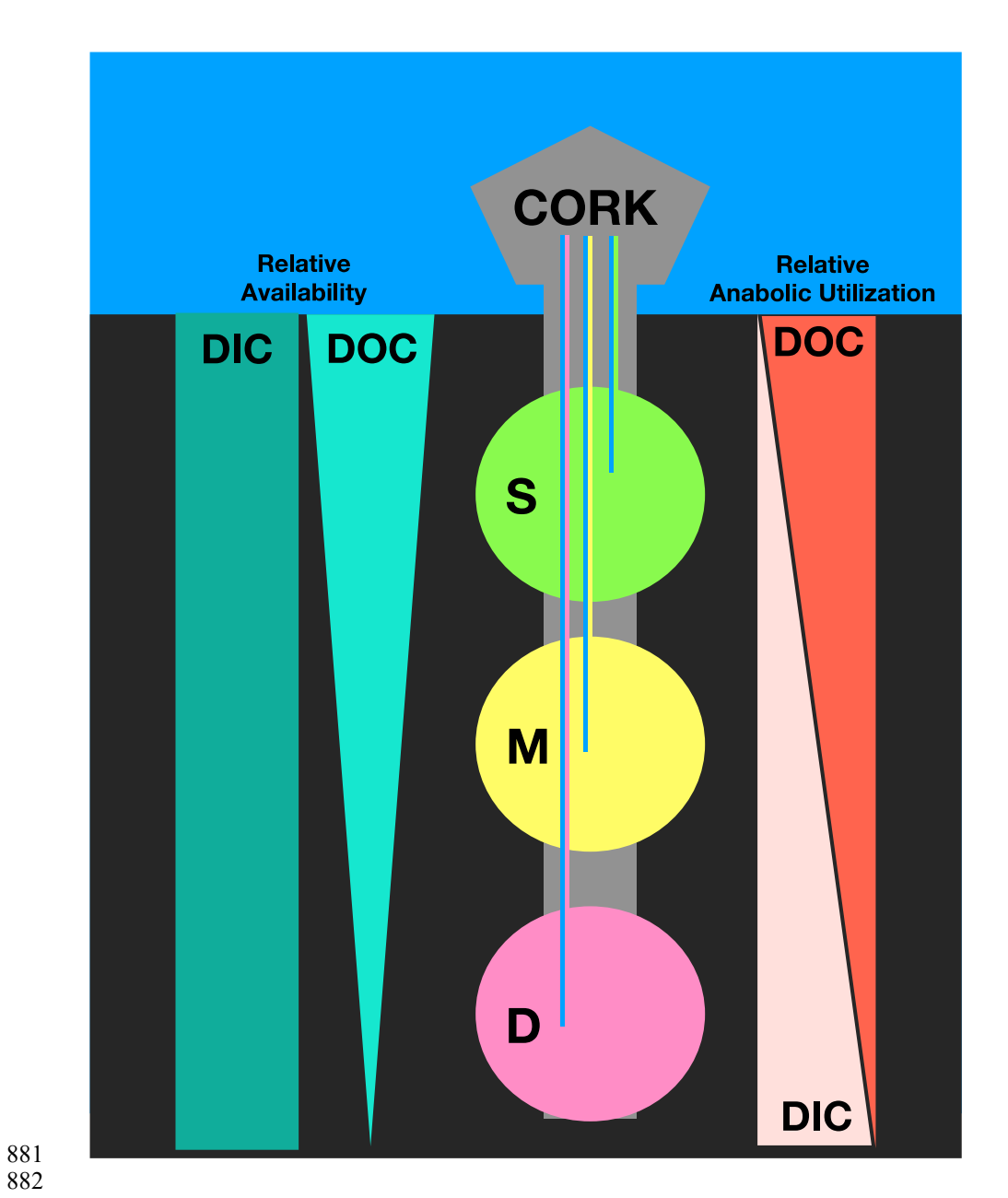


Fig. S8. A schematic representation of the relative availably and anabolic utilization of DOC compared to DIC with depth in North Pond crustal fluids as a strategy to reduce reliance on a winnowing and aging DOC pool.

Science Advances

883

884

GFF blanks	С µg	C µmol	Run Date				
U1382A TP3 Blank	5.93	0.49	19-Feb	Avg	Stdev	Avg+std	Max
U1383C-M Blank	7.48	0.62	19-Feb	0.56	0.09	0.65	0.62
11 blank	6.84	0.57	May-19				
22 blank	6.51	0.54	May-19				
33 blank	5.80	0.48	May-19	0.53	0.04	0.58	0.57
23 blank	5.93	0.49	Apr-19				
M blank	7.48	0.62	Apr-19				
44 blank	5.04	0.42	Apr-19				
55 blank	6.48	0.54	Apr-19				
64 blank	4.13	0.34	Apr-19	0.48	0.11	0.59	0.62

Capsule Blanks	μg C	Run Date
No Canaula	0.16 +/-	
No Capsule	0.15	Mar-19
Empty Sp Capaula	1.16 +/-	
Empty Sn Capsule	0.12	Mar-19
	1.57 +/-	
NH4(SO4)2	0.56	Apr-19

Polycarbonate Blanks	δ ¹³ C vs. PDB	C µmol	δ ¹⁵ N vs. AIR	N µmol
Filter 1	-27.76	96.47	-2.43	0.72
Filter 2	-27.71	100.3 8	-5.17	0.75

Table S1.

GFF filter and capsule blanks for Elemental Analysis and polycarbonate filter blanks for NanoSIMS background correction.

Science Advances Manuscript Template Page 33 of 37

Sample	Time Point (d)	Atom% ¹³ C	С µg	C µmol	F _{inital}
Bottom	6	1.0869	14.87	0.59	0.01087
U1383C-Shallow	6	1.0864	14.30	0.54	0.01086
U1383C-Middle	6	1.0872	26.42	1.55	0.01087
U1382A	6	1.0892	28.62	1.73	0.01089
U1383C-Middle	2	1.0870	19.65	1.05	0.01087
U1383C-Deep	2	1.0756	22.63	1.29	0.01076
				Avg.	0.01085
				Stdev.	0.00005

Table S2.

Bulk elemental analysis filters from Condition 1 samples with no carbon or nitrogen isotope added used to calculate natural abundance biomass for isotope mass balance equations.

Science Advances Manuscript Template Page 34 of 37

Tracer	Added (µM)	Added (µmol)	Background (µM)	Background (µmol)	In situ (µmol)	F _{label}
Tracer	(pivi)	(ріпоі)	(pivi)	(ріноі)	302-	■ label
Bicarbonate(C)*	200	28.8	1940-1970	279-284	313	0.1^
Acetate (C)	1.5	0.216	1.500	0.2	0.4	0.50
Methylamine (C)	4	0.576	1.500	0.2	0.8	0.73
Diatom Lysate (C)	2	0.288	1.500	0.2	0.5	0.57
Methylamine (N)	4	0.576	0.0055	0	0.6	0.99
Diatom lysate (N)	0.6	0.086	0.0055	0	0.1	0.99
Ammonium (N)	0.01	0.00144	0.0055	0	0.002	0.64

Table S3.

 Estimated isotope label fractional abundance for incubation isotope mass balance calculations. *Background DIC concentrations differ from in situ with 5 ml dilution from $^2\mathrm{H}_2\mathrm{O}$ addition. ^See supplemental methods for calculation.

Science Advances Manuscript Template Page 35 of 37

		1	T	1	1	
		Published			pmol	
	Labeled Substrate	Values	Location	Тетр	ml ⁻¹ d ⁻¹	Ref.
S	¹³ C-MeAm	-	2017 fluids	4°C	bd-17	this study
nd	¹³ C-MeAm	-	2017 fluids	20°C	bd-72	this study
no	¹³ C-Urea	0.2-0.5 nmol/L/h	50-75m N. Pacific ODZ	in situ	5-12	(36)
spunodwoo	¹³ C-Cyn.	0.1-0.6 nmol/L/h	50-75m N. Pacific ODZ	in situ	2-14	(36)
00	¹⁵ N-Urea	0.3-10 nmol/L/h	50-75m N. Pacific ODZ	in situ	7-233	(36)
S	¹⁵ N-Cyn.	0.3-0.1 nmol/L/h	50-75m N. Pacific ODZ	in situ	2-7	(36)
0	¹⁵ N-Am.	0.2-11 nmol/L/h	50-75m N. Pacific ODZ	in situ	5-264	(36)
	¹³ C-DIC	-	2017 fluids	4°C	bd-78	this study
	¹³ C-DIC	-	2017 fluids	20°C	bd-94	this study
	¹³ C-DIC	856 pmol/ml/d	North Pond Bottom Water	5°C	856	(8)
드	¹³ C-DIC	1334 pmol/ml/d	North Pond Bottom Water	25°C	1334	(8)
Carbon	¹³ C-DIC	1332 pmol/ml/d	North Pond U1382A	5°C	1332	(8)
Ca	¹³ C-DIC	3742 pmol/ml/d	North Pond U1382A	25°C	3742	(8)
	¹³ C-DIC	3031 pmol/ml/d	North Pond U1383C Shallow	5°C	3031	(8)
norganic	¹³ C-DIC	3277 pmol/ml/d	North Pond U1383C Shallow	25°C	3277	(8)
org	¹³ C-DIC	322 pmol/ml/d	North Pond U1383C Deep	5°C	322	(8)
Ľ	¹³ C-DIC	4328 pmol/ml/d	North Pond U1383C Deep	25°C	4328	(8)
	¹⁴ C-DIC	0.24 umol/m ³ /d	NADW 2537 m	in situ	0.24	(24)
	¹³ C-DIC	50 ug C/L/d	EPR, pressurized, bulk rate	24°C	4167	(14)
	¹³ C-DIC+110 μM O ₂	100 ug C/L/d	EPR, pressurized, bulk rate	24°C	8333	(14)
	¹³ C-Acetate	-	2017 fluids	4°C	bd-57	this study
	¹³ C-Acetate	-	2017 fluids	20°C	bd-700	this study
_	¹³ C-Acetate	26 pmol/ml/d	North Pond Bottom Water	5°C	26	(8)
Carbon	¹³ C-Acetate	28 pmol/ml/d	North Pond Bottom Water	25°C	28	(8)
Sar	¹³ C-Acetate	58 pmol/ml/d	North Pond U1382A	5°C	58	(8)
00	¹³ C-Acetate	104 pmol/ml/d	North Pond U1382A	25°C	104	(8)
Organic (¹³ C-Acetate	95 pmol/ml/d	North Pond U1383C Shallow	5°C	95	(8)
rg	¹³ C-Acetate	87 pmol/ml/d	North Pond U1383C Shallow	25°C	87	(8)
0	¹³ C-Acetate	6 pmol/ml/d	North Pond U1383C Deep	5°C	6	(8)
	¹³ C-Acetate	69 pmol/ml/d	North Pond U1383C Deep	25°C	69	(8)
	¹⁴ C-Leucine	0.88 umol/m3/d	NADW 2537 m	in situ	0.88	(24)

Table S4. Bulk stable and radioisotope-based reference literature value conversions for comparison to 2017 results.

Science Advances Manuscript Template Page 36 of 37

913 914

915916

917

918

919

920921922

Labeled C	Published	fmol cell ⁻¹ d ⁻¹	Labeled N	Published	fmol cell ⁻¹ d ⁻¹	Location	Ref.
Substrate	values		Substrate	values			
¹³ C-Acetate	2.17x10 ⁻¹⁷	0.0217	¹⁵ N-	2.09 x10 ⁻¹⁷	0.0209	219 mbsf	(11)
	mol cell ⁻¹ d ⁻¹		Ammonium	mol cell ⁻¹ d ⁻¹		sediment	
¹³ C-DIC	6.73x10 ⁻¹⁷	0.0673	¹⁵ N-	1.77x10 ⁻¹⁷	0.0177	219 mbsf	(11)
	mol cell ⁻¹ d ⁻¹		Ammonium	mol cell ⁻¹ d ⁻¹		sediment	
¹³ C-DIC	17.00	2.8*	-	-	-	EPR vent	(14)
	μg C L ⁻¹ d ⁻¹					fluids	
¹³ C-DIC+	80	13.3*	-	-	-	EPR vent	(14)
110 µM O ₂	μg C L ⁻¹ d ⁻¹					fluids	

^{*}assuming 5x10⁵ cells per ml (14)

Table S5.

Single cell NanoSIMS-based reference literature value conversions for comparison to 2017 results.

Dataset S1 (separate file). Incubation cell counts.

Dataset S2 (separate file). Bulk EA carbon incorporation rates.

Dataset S3 (separate file). NanoSIMS ROI fractional abundance and estimated carbon and nitrogen incorporation rates.

Science Advances Manuscript Template Page 37 of 37